



Article Information

Submitted: May 30, 2024

Approved: July 15, 2024

Published: July 16, 2024

How to cite this article: Ronald SO. Lattice Boltzmann Method without Invoking the $M \ll 1$ Assumption. IgMin Res. July 16, 2024; 2(7): 589-610. IgMin ID: igmin223; DOI: 10.61927/igmin223; Available at: igmin.link/p223

Copyright: © 2024 Ronald SO. This is an open access article distributed under the Creative Commons Attribution License, which permits unrestricted use, distribution, and reproduction in any medium, provided the original work is properly cited.

Keywords: Maxwellian distribution; Euler equations; Navier-stokes equations; Aeroacoustics simulation

Review Article



Lattice Boltzmann Method without Invoking the $M \ll 1$ Assumption

SO Ronald*

RMC So Department of Mechanical Engineering, The Hong Kong Polytechnic University, Hung Hom, Kowloon, HKSAR, PRC, Hong Kong

***Correspondence:** SO Ronald, RMC So Department of Mechanical Engineering, The Hong Kong Polytechnic University, Hung Hom, Kowloon, HKSAR, PRC, Hong Kong, Email: ronald.so@polyu.edu.hk



Abstract

When a Maxwellian distribution is assumed for the distribution function in the BGK-type modelled BE, it will give rise to the Euler equations if it is the first-order approximation in the Chapman-Enskog method. Then the second-order equations will yield the N-S equations. Most LBM developed to date are formulated based on the second-order equations. Consequently, the assumption of a flow Mach number $M \ll 1$ is inherent in this formulation. This approach creates an unnecessary restriction on the LBM that should be avoided if possible. An alternative approach is to formulate a new LBM by considering an equilibrium distribution function where the first-order approximations give rise to the N-S equations. Adopting this approach, a new LBM has been formulated. This new LBM gives reliable results when applied to simulate aeroacoustics, incompressible flows, and compressible flows with and without shocks. Good agreement with measurements and numerical data derived from DAS/DNA calculations is obtained.

Nomenclature

BE: Boltzmann Equation; BGK: Bhatnagar, Gross and Krook; c^p : Specific Heat of Fluid; D: Dimension of the Problem; DAS: Direct Aeroacoustics Simulation; DNS: Direct Numerical Simulation; D_{\perp} : Translational Degree-of-freedom; D_{\parallel} : Rotational Degree-of-freedom; e : Internal Energy of Fluid; e_t : Total Energy; f : Dimensionless Particle Distribution Function; f^{eq} : Equilibrium Distribution Function; Kn: Knudsen number; L : Characteristic Length Scale; LBM: lattice Boltzmann Method; M : Mach Number; MBE: Modelled Boltzmann Equation; N-S: Navier-Stokes; p : Pressure; Pr: Prandtl Number; q_j : Heat Flux Vector; R : Universal Gas Constant; Re: Reynolds Number; SRT: Single-relaxation-time; T : Temperature; t : Time; U : Characteristic Velocity Scale; u : Velocity Along x-direction; v : Velocity Along y-direction; WCUB: Wang-Chang, Uhlenbeck, and DeBoer; x : x-coordinate; y : y-coordinate

Symbols

α : Lattice Velocity Index; γ : Specific Heat Ratio; κ : Coefficient of Thermal Conductivity; μ : Coefficient of Viscosity; ξ : Dimensionless Particle Velocity Vector; ρ : Fluid Density; σ_{ij} : Viscous Stress Tensor; τ : Particle Collision Relaxation Time or Non-dimensional Relaxation Time; τ_c : Mesoscopic Time Scale; τ_{ij} : Stress Tensor

Superscripts and subscripts

\wedge : Superscript for Dimensional Value; r : Subscript for Reference Condition; t : Subscript for Total Condition

Introduction

It has been established that if the Knudsen number (Kn) is used as an expansion parameter, the Navier-Stokes (N-S) equations and their transport coefficients can be derived from the Boltzmann Equation (BE) using the Chapman-Enskog or multi-scale expansion [1]. Consequently, for hydrodynamic and fluid dynamic flow problems in the continuum regime, with $\text{Kn} \ll 1$ assumed, solving the BE provides an alternative and a more fundamental approach other than directly solving the N-S equations [2-6]. However, due to the complexity of the BE and the difficulty involved in solving it, attempts have been made by different researchers to simplify the BE through modeling. Among them, a commonly accepted model was that suggested by Bhatnagar Gross and Krook [7], hereafter designated as the BGK model. The BGK model was proposed for monatomic gas, where the gas particles were assumed to be rigid spheres with only the translational degree of freedom considered in analyzing the collision dynamics. Thus, a Maxwellian distribution is assumed for the equilibrium distribution function f^{eq} in the BGK model. Since then, most



studies on the modeled BE were carried out by invoking the monatomic gas assumption, because work on polyatomic gas would involve a generalization of the modeled BE to include as many energy modes as mathematically possible.

When rotational angular momentum is also considered in the derivation of f^{eq} , the resulting theory could be quite complicated, especially for numerical simulations. Wang-Chang, et al. [3] suggested a WCUB equation by introducing a set of particle distribution function f for each quantum mode to specify the internal state of the particles. Their equation is based on a spherically symmetric inter-particle potential, and it yields an appropriate description for polyatomic gas. However, their formulation does not consider the polyatomic gas with significant dipole moments or with a degenerating internal state [7]. This is in spite of the fact that the degenerate rotational states do play an important role in angular momentum polarizations. Nevertheless, the WCUB equation has been used by other researchers as a base to formulate simpler models; a good example is the approach of Morse [4] who simplified the WCUB equation using a BGK-type modelled BE.

Different numerical methods have been used to solve the BGK-type modelled BE. Among the more widely used methods were those put forward by Broadwell [8], Cao, et al. [9], Mei and Shyy [10], and Wolf-Gladrow [11]. The method of Broadwell [8] is a discrete velocity method and assumes that the gas particles can be restricted to having only a small number of velocities. The classical lattice Boltzmann method (LBM) or finite difference-based lattice Boltzmann method (FDLBM), such as those proposed by Cao, et al. [9] and Mei and Shyy [10], fall into this category. On the other hand, LBM is a special example of a particular discretization of the discrete Boltzmann equation [11].

In the initial stage of development of the LBM, there was a common understanding that the transport coefficients, such as the first coefficient of viscosity μ , the coefficient of thermal conductivity κ , and the ratio of specific heats γ , could be correctly recovered from the modelled BE. In order to achieve these objectives, a small Mach number assumption, $M \ll 1$, was found to be necessary. This assumption is a consequence of the Taylor expansion invoked for the continuous f^{eq} because it facilitates the derivation of the lattice counterpart. Unfortunately, this approach limits the application of the method to incompressible flow subject to a Mach number restriction of $M \ll 1$. This assumption renders the energy equation no part to play in the whole formulation. On the other hand, recovery of the N-S equations for monatomic gas using the Chapman-Enskog expansion in continuous form supports the possibility of inclusion of the energy equation and its application to compressible flows. Consequently, Alexander, et al. [12] proposed a thermal LBM with the energy equation

included, while McNamara and Alder [13] showed that LBM could be made to mimic the thermal N-S equations by fixing a number of moments of the f^{eq} . Even though improvements along these lines have been made, incorrect predictions of gas properties, such as the ratio of specific heats γ , the Prandtl number Pr , etc. still occur in the commonly used LBM and are restricted to monatomic gas only. Most shortcomings can be traced to the original BGK model. Therefore, conventional LBM can be improved by first taking a critical, yet succinct, analysis of the originally assumed BGK model.

Numerous attempts have been made by different researchers to remedy the monatomic gas restriction in the LBM approach; these include the concept of multi-energy level to facilitate a flexible specific-heat ratio, such as those suggested by Cao, et al. [9], Hu, et al. [14] and Kataoka and Tsutahara [15], and the proposal of Xu [16] to modify the Maxwellian equilibrium distribution function by introducing an internal velocity associated with certain number of internal degrees of freedom to develop a gas kinetic scheme. Thus, the scheme will no longer be restricted to the field of the discrete velocity method. In principle, these schemes are also suitable for diatomic and polyatomic gases. An alternative approach for diatomic gas alone has been put forward by Li, et al. [17], where the rotational degree of freedom of the gas particles is also considered in a modified definition of the total energy. Their approach leads to a slightly different f^{eq} , the Maxwellian distribution. The modified f^{eq} of Li, et al. [17] is not limited to FDLBM, even though they used FDLBM to solve aeroacoustics problems to demonstrate the validity and viability of the proposed approach for diatomic gas.

In the BGK-type modelled BE, a unity Prandtl number, $Pr = (\mu_r c_{p,r})/\kappa_r = 1$, is inherent in the formulation even when μ is correctly recovered as demonstrated by Li, et al. [17] and Li [18]. Here, c_p is the specific heat of the fluid at constant pressure and the subscript r in $c_{p,r}$, μ_r , and κ_r refers to the reference condition. This incorrect $Pr = 1$ suggests that the thermal energy exchange between particles has not been replicated properly. Attempts to recover Pr correctly have been made; a well-known attempt is the BGK-Ellipsoidal-Statistical model of Holway [6] which replaces the Maxwellian equilibrium distribution function of the original BGK model with an anisotropic Gaussian distribution. The proposal of Holway [6] has one drawback though; it is not easily adapted to numerical schemes. Since then, more practical methods have been put forward; they include the multiple relaxation time approach and Eucken's [19] theory of heat conduction for gas particles.

One of the reasons for the incorrect $Pr = 1$ value could be attributed to the Single-Relaxation-Time (SRT) model assumed in the BGK-type modelled BE of Lallemand and Luo [20]. Under the SRT model, the additional time required for

the relaxation of thermal energy after collision is neglected. In view of this, attempts have been made to extend the BGK-type modelled BE to solve thermal problems based on a multi-speed and multi-relaxation time model. Alexander, et al. [12] proposed a two-dimensional (2-D) thermal LBM for monatomic gas. However, the resulting Pr thus obtained has a value of 0.5 which is inconsistent with real gas. Chen, et al. [21] employed a higher-order velocity expansion for the f^{eq} to correct the calculated viscous stress and heat flux; however, details of the parameter's construction were not provided. Multi-speed and dual relaxation rate models proposed by McNamara, et al. [22], and Teixeira, et al. [23] allowed variation of Pr but their models are numerically unstable. Furthermore, the stabilization methods proposed in their approach were quite ad hoc. Lallemand and Luo [20] decoupled the shear and energy modes of the linearized evolution operator to improve its numerical stability but did not elaborate on the physical background of the proposed approach. A passive scalar approach by Shan [24] introduced an additional distribution function to help solve the energy equation separately. The proposed thermal LBM model led to a much higher computational cost compared to the isothermal case. Adopting the modified BGK-type modelled BE proposed by Li, et al. [17], Leung, et al. [25] were able to show that the correct Pr can be recovered from an application of Eucken's [19] theory of heat conduction to this approach. Unfortunately, no simulations have been carried out to validate the proposed concept and approach. Together, these studies show that the BGK-type modelled BE needs further improvement if the thermal energy exchange during the collision were to be sufficiently accounted for to enable a correct recovery of Pr.

It is clear that, besides the required assumption of a very small Kn for the recovery of the continuum transport equations, the BGK-type modelled BE examined so far shares two more common grounds. These are the assumption of a Maxwellian distribution (or its slight variation) for f^{eq} in the BGK model, and the expectation that the BGK-type modelled BE should not only recover the continuum transport equations but also the transport properties of the fluid, such as μ and κ , or their non-dimensional equivalent, Re and Pr. Here, Re is the Reynolds number defined as $Re = \rho_r U_r L / \mu_r$, and Pr is the Prandtl number previously given as $Pr = (\mu_r c_{pr}) / \kappa_r = 1$. In these expressions, U is the characteristic velocity scale, L is the characteristic length scale, and ρ is the fluid density. Since this latter point is known to be the case in the original BE, researchers often reasoned that particle collision physics could be sufficiently accounted for in the f^{eq} and in the yet-to-be-defined particle collision relaxation time τ in the BGK model to effect correct recovery of fluid properties. Consequently, this assumption has been commonly invoked in subsequent work carried out to date.

As pointed out by Aristov [26], the distribution function

in the BGK-type modelled BE takes a certain form. The Maxwellian distribution gives rise to the Euler equations if it is the first-order approximation in the Chapman-Enskog method, then the second-order equation would yield the N-S equations, while the fluid transport coefficients can be tied to τ . The LBM thus derived is restricted by two assumptions; these are a monatomic gas and a flow Mach number $M \ll 1$. The first assumption can be addressed by reformulating an f^{eq} for diatomic gas [27]. On the other hand, the second assumption, besides being restrictive in M , can also lead to leakage at the wall and in the computational domain of incompressible flow [27]. Without corrections, the leakage will eventually compromise the calculated velocity field, thus leading to a situation where the continuity equation is no longer satisfied. Some remedies to the conventional LBM have been implemented; however, the monatomic gas and the $M \ll 1$ assumption discussed above still have not been properly addressed. The monatomic gas assumption can be dealt with by reformulating the f^{eq} for diatomic gas. As for $M \ll 1$, it is helpful to note that the LBM thus derived is essentially obtained from the second-order terms in the distribution function assumed, thus giving rise to this $M \ll 1$ assumption. If a distribution function can be formulated such that the first-order terms can give rise to the N-S equations, then the resultant LBM will be free of the $M \ll 1$ assumption. Therefore, it is appropriate to ask if this $M \ll 1$ assumption is necessary or can be relaxed or replaced by improving the existing model of the BE.

From the above discussion, it is clear that assuming a BGK-type model for the BE is appropriate, but not entirely correct. Therefore, improvements in the Maxwellian distribution and its variation invoked for f^{eq} can be sought. This approach has been demonstrated to be valid for the case of exact recovery of the Euler equations by Fu, et al. [28] and So, et al. [29], and they have derived an alternate f^{eq} where the first term is given by a Maxwellian distribution. Three additional terms partially modeling the physics of particle-particle collision are also present. This enables an alternative f^{eq} along the line suggested by So, et al. [30] to be sought with an objective to sufficiently account for the particle-particle collision physics to recover the N-S equations in a first-order Kn expansion of the modelled BE. Thus formulated, a new LBM free of the two commonly made assumptions is available. In addition, it is anticipated that the N-S equations recovered from the particle relaxation time τ would not be arbitrary. Rather, its determination can be shown to be related to the scaling chosen to render the modelled BE dimensionless. With these modifications, $Kn \ll 1$ is the only assumption left in the proposed approach to formulate a new LBM.

Objectives

The present study serves as a further explanation and, at the same time, provides supplemental information to previous

work [30] on the formulation of a general f^{eq} that is valid and equally applicable for incompressible and compressible flows. The continuum N-S equations required specifications of the fluid transport coefficients either in their dimensional form or as dimensionless numbers M , Pr , Re , etc. It is reasonable to allow the same specifications for the recovered N-S equations from the modelled BE. Therefore, the reference M , Pr , Re , etc. are considered as free parameters to be specified, instead of being a part of the solution of the modelled BE.

The f^{eq} will be constructed in such a way that only first-order approximation terms are needed to recover the N-S equations; thus the $M \ll 1$ assumption is not needed in this approach. Once the continuous f^{eq} is obtained, its lattice counterpart can be derived and proposals for a two-dimensional (2-D) improved LBM can be put forward. Validations of the improved LBM are carried out against aeroacoustics and diatomic gas flow studies with M varying from $M \ll 1$ to $M > 1$. Special attention is paid to the resolution of shock structures for all $M > 1$ flows considered. The calculations are validated against available experimental, analytical, direct numerical (DNS), and Direct Aeroacoustics (DAS) simulation results. To demonstrate the validity and viability of the new f^{eq} thus derived, most cases considered previously in [30] are again chosen as test cases for the present paper.

It is expected that the present paper shares certain common mathematical formulations with So, et al. [30]. However, to facilitate an easy understanding of the methodology and formulation used to derive the improved LBM, it is necessary to give a stand-alone derivation of the improved LBM in Section 3 below.

Recovery of the Navier-stokes equations

Governing equations: The basis of the present analysis is the acoustics scaling form of the N-S equations for a compressible gas. According to Lele [31], these equations can be written as:

$$\frac{\partial \rho}{\partial t} + \frac{\partial \rho u_i}{\partial x_i} = 0 \tag{1}$$

$$\frac{\partial \rho u_i}{\partial t} + \frac{\partial \rho u_i u_j}{\partial x_j} = - \frac{\partial p}{\partial x_i} + \frac{M}{Re} \frac{\partial \sigma_{ij}}{\partial x_j} \tag{2}$$

$$\frac{\partial \rho e_t}{\partial t} + \frac{\partial \rho u_i e_t}{\partial x_i} = - \frac{\partial p u_i}{\partial x_i} + \frac{M}{Re} \frac{\partial \sigma_{ij} u_i}{\partial x_j} - \frac{M}{RePr} \frac{\partial q_i}{\partial x_i} \tag{3}$$

$$p = \rho RT / c_p \tag{4}$$

Where the total energy e_t is defined as $e_t = e + (1/2|u|^2)$. The viscous stress tensor σ_{ij} and the heat flux vector q_i are given by

$$\sigma_{ij} = 2\mu \left(S_{ij} - \frac{1}{3} \delta_{ij} S_k \right) \text{ where } S_{ij} = \frac{1}{2} \left(\frac{\partial u_i}{\partial x_j} + \frac{\partial u_j}{\partial x_i} \right) \tag{5a,b}$$

$$q_i = -\kappa \frac{\partial T}{\partial x_i} \tag{6}$$

Here, t is time, x_i is the position vector, u_i is the velocity vector, p is pressure, ρ is density, e is the internal energy of the fluid, T is its temperature, and R is the Universal gas constant. These symbols are used to denote dimensionless variables while their dimensional counterparts are designated by the same symbols with a hat (^). The equations are derived using the characteristic scaling for length L , velocity c_r , time L/c_r , density ρ_r , pressure $\rho_r c_r^2$, temperature c_r^2/c_p , total energy c_r^2 , viscosity μ_r , and conductivity κ_r . With these scaling, the following dimensionless parameters can be defined: $M = U_r/c_r$, $Re = \rho_r L U_r / \mu_r$, $Pr = \mu_r c_{pr} / \kappa_r$, $\mu = \hat{\mu} / \mu_r$, $\kappa = \hat{\kappa} / \kappa_r$. Here, U_r is the reference velocity. Finally, it should be pointed out that in writing down Eqs. (1) to (6), bold face and indices are used interchangeably to denote a vector, while only indices are used to denote second-order tensors, and repeated indices represent summation over the order of the tensor.

The objective of the present study is to attempt a recovery of the N-S equations as given in Eqs. (1) – (4) from a modelled form of the Boltzmann equation (MBE). The vehicle chosen is the BGK-type modelled BE with an unknown equilibrium distribution function \hat{f}^{eq} , and an undefined particle collision relaxation time $\hat{\tau}$. This BGK-typed MBE in dimensionless form can be written as

$$\frac{\partial f}{\partial t} + \xi \cdot \nabla_x f = - \frac{1}{\tau Kn} (f - f^{eq}) \tag{7}$$

In Eq. (7), f is the dimensionless particle distribution function, ξ is the dimensionless particle velocity vector, and τ is the non-dimensional relaxation time. Acoustics scaling has been used to make the equation dimensionless with normalization for $\hat{\tau}$, \hat{f} and \hat{f}^{eq} given by

$$\tau = \frac{\hat{\tau}}{\tau_o} \tag{8a}$$

$$f, f^{eq} = \frac{\hat{f}, \hat{f}^{eq}}{\rho_r / c_r^D} \tag{8b}$$

Where $\tau_o = LKn/c_r$ is the mesoscopic time scale, Kn is defined by $Kn = x_o/L$, x_o is the mesoscopic length scale, and D is the dimension of the problem (2 for 2-D and 3 for 3-D flows). It is assumed that the length scale x_o is very small compared to L , i.e., $x_o \ll L$; therefore, both Kn and τ_o are very small. Note that under this normalization, τKn appears together and later simulations using LBM will show that as long as $Kn \ll 1$, there is no loss of generality to assume τ to be of order one.

This BGK-typed MBE assumes that the nonlinear particle collision behavior embodied in the collision integral of the original BE [30] has been sufficiently modelled in f^{eq} , and that the deviation of f from its equilibrium state is small; therefore, f could be determined by solving Eq. (7) alone. The fact that the deviation of f from f^{eq} is small has been assumed by other

researchers to demonstrate that the continuum Euler and N-S equations can be recovered from Eq. (7), albeit not exactly, provided the dense gas assumption is invoked. In other words, inherent in their approach $Kn \ll 1$ has also been assumed. Under this assumption, f can be expanded in terms of Kn to give

$$f = f^{(0)} + Kn f^{(1)} + Kn^2 f^{(2)} + \dots \quad (9)$$

Substituting Eq. (9) into Eq. (7) and collecting the same order terms to $O(Kn^2)$ gives the following equations for the first three elements of $f^{(i)}$; they are

$$f^{(0)} = f^{eq} \text{ to } O(Kn^0) \quad (10)$$

$$\frac{\partial f^{(0)}}{\partial t} + \xi \cdot \nabla_x f^{(0)} = -\frac{f^{(1)}}{\tau} \text{ to } O(Kn^1) \quad (11)$$

$$\frac{\partial f^{(1)}}{\partial t} + \xi \cdot \nabla_x f^{(1)} = -\frac{f^{(2)}}{\tau} \text{ to } O(Kn^2) \quad (12)$$

The original BGK model was proposed for monatomic gas, therefore, only the translational degree-of-freedom D_T of the particle was considered, and f is given by a Maxwellian distribution. Consequently, the specific heat ratio γ recovered for a diatomic gas is incorrect. It has been shown by Li, et al. [17] that $\gamma = 1.4$ for diatomic gas can be recovered exactly if the rotational degree-of-freedom D_R of the particles is also included in the definition of the total energy, e_t . In order to recover Eqs. (1) – (4) correctly for diatomic gas, the following macroscopic constraints have to be satisfied by f^{eq} and its moments in the particle velocity space. These constraints are given by:

$$\rho = \int f^{eq} d\xi \quad (13)$$

$$\rho u_i = \int f^{eq} \xi_i d\xi \quad (14)$$

$$\rho e_t = \rho e + \frac{1}{2} \rho |u|^2 = \frac{D_T + D_R}{D} \int \frac{1}{2} f^q |\xi|^2 d\xi \quad (15)$$

Higher-order terms $f^{(n)}$ and their moments are given by

$$\int f^{(n)} d\xi = 0 \quad (16a)$$

$$\int f^{(n)} \xi d\xi = 0 \quad (16b)$$

$$\frac{D_T + D_R}{D} \int \frac{1}{2} f^{(n)} |\xi|^2 d\xi = 0 \text{ for all } n \geq 1 \quad (16c)$$

A slightly different way of writing Eq. (15) could better explain the physics of the e_t definition. This alternate form is

$$\rho e_t = \rho e + \frac{1}{2} \rho |u|^2 = \frac{D_T + D_R}{D} \int \frac{1}{2} f^q |\xi|^2 d\xi + \int \frac{1}{2} f^q |\xi - u|^2 d\xi + \frac{\hat{E}}{D} \int \frac{1}{2} f^q |\xi|^2 d\xi + \frac{1}{2} \rho |u|^2 \quad (17)$$

Where $(\xi - u)$ is the peculiar velocity of the particles and $K = D_T + D_R - D$ is the number of internal degrees of freedom. The first term on the right-hand side of Eq. (17) is the internal energy derived from the translational motion of the particles, while the second term accounts for the rotational motion,

and the third term represents the kinetic energy of the flow. If the ideal gas law as given in Eq. (4) were to be recovered identically, this requires that $p = \rho \theta$, where $\theta = RT/c_p$ has been assumed, and the equi-partition theorem would then yield

$$e = \frac{D_T + D_R}{2} \theta = \frac{\theta}{\gamma - 1} \text{ with } \gamma \text{ defined by } \gamma = \frac{D_T + D_R + 2}{D_T + D_R} \quad (18)$$

This leads to a correct expression for e and an expression for γ that does not depend on D . Consequently, $\gamma = 1.4$ is recovered correctly for any D because $D_T = 3$ and $D_R = 2$.

Once the equation of state has been recovered identically, the next step is to recover Eqs. (1) – (3). This is accomplished by multiplying Eq. (11) by $\{1, \xi, (\xi^2/2)(D_T + D_R)/D\}$ and then integrating over the whole particle velocity space. Making use of Eq. (10) and Eqs. (13) – (16), the following equations are obtained,

$$\int \left[\frac{\partial f^{eq}}{\partial t} + \frac{\partial}{\partial x_j} (\xi_j f^{eq}) = -\frac{f^{(1)}}{\tau} \right] d\xi \Rightarrow \frac{\partial \rho}{\partial t} + \frac{\partial}{\partial x_j} (\rho u_j) = 0 \quad (19)$$

$$\int \left[\frac{\partial f^{eq}}{\partial t} + \frac{\partial}{\partial x_j} (\xi_j f^{eq}) = -\frac{f^{(1)}}{\tau} \right] \xi_i d\xi \Rightarrow \frac{\partial (\rho u_i)}{\partial t} + \frac{\partial}{\partial x_j} (\int \xi_i \xi_j f^{eq} d\xi) = 0 \quad (20)$$

$$\int \left[\frac{\partial f^{eq}}{\partial t} + \frac{\partial}{\partial x_j} (\xi_j f^{eq}) = -\frac{f^{(1)}}{\tau} \right] \frac{|\xi|^2}{2} \left(\frac{D_T + D_R}{D} \right) d\xi \Rightarrow \frac{\partial (\rho e_t)}{\partial t} + \frac{\partial}{\partial x_j} \left(\int \frac{D_T + D_R}{D} \xi_j \frac{|\xi|^2}{2} f^{eq} d\xi \right) = 0 \quad (21)$$

Up to this point, the derivation follows the conventional approach which assumes that the Euler equations can be recovered from the expanded MBE for $f^{(1)}$, while the N-S equations would need the additional consideration of the expanded MBE for $f^{(2)}$. Furthermore, it has been argued that the transport coefficients associated with the N-S equations, such as μ, κ , etc., should be related to τ and could be recovered from the MBE. This is the approach adopted here.

Another approach could be built on the assumption that it is not necessary to attempt to recover the transport coefficients from the MBE and to tie them to τ . After all, the continuum N-S equations to be recovered assume that these transport coefficients are known and can be specified in the form of non-dimensional numbers. Since only the MBE is solved and not the original BE, there are no convincing arguments to justify the assumption that the same physics embodied in the original BE can be replicated in its entirety in the BGK-type MBE. Eqs. (1) – (3) can be recovered from Eqs. (19) – (21) by permitting the reference non-dimensional numbers, such as M, Re , and Pr , to be specified. This, however, does not preclude their local values from being determined in the course of solving the BGK-type MBE. Of course, the validity of this assumption will have to be justified; one way to do so is to compare the MBE simulations with either the theoretical solutions, if available, or with numerical results obtained by directly solving the N-S equations.

Once this assumption is invoked, recovery of Eqs. (1) – (3) from Eqs. (19) – (21) leads to the following identities for the integral terms in Eqs. (20) and (21).

$$\int (\xi_i)(\xi_j) f^a d\xi = p\delta_j + \rho u_i u_j + \tau_j + P'_j \quad (22)$$

$$\int \frac{D_T + D_R}{D} \xi_j \frac{|\xi|^2}{2} f^a d\xi = u_j(p + \rho e_i) + (q_j + u_k \tau_k) + Q'_j \quad (23)$$

Where τ_{ij} is the stress tensor and together with the vector q_j have to be specified. The unknown second-order tensor P'_{ij} and vector Q'_j can now be determined once τ_{ij} and q_j are defined. Therefore, equations governing the behavior of P'_{ij} and Q'_j are required. It can be seen that Eq. (2) can be recovered exactly if τ_{ij} is defined as

$$-\tau_{ij} = \frac{M}{\text{Re}} \sigma_{ij} = \frac{M}{\text{Re}} 2\mu \left(S_{ij} - \frac{1}{3} \delta_{ij} S_{kk} \right) \quad (24)$$

And P'_{ij} satisfies the condition

$$\frac{\partial P'_{ij}}{\partial x_j} = 0 \quad (25)$$

Similarly, Eq. (3) can be recovered exactly if q_j is defined as

$$q_j = \frac{M}{\text{PrRe}} \left(-\kappa \frac{\partial T}{\partial x_j} \right) \quad (26)$$

And Q'_j satisfies the condition

$$\frac{\partial Q'_j}{\partial x_j} = 0 \quad (27)$$

The exact recovery of the N-S equations, therefore, hinges on the determination of P'_{ij} and Q'_j , which are governed by Eqs. (25) and (27), and an evaluation of the unknown function f^{eq} .

Before proceeding to determine f^{eq} , P'_{ij} and Q'_j , it should be noted that, according to their definitions, M , Re , and Pr are evaluated at the reference point, i.e., they are not the local M , Re , and Pr . In a flow where μ and κ do not vary much with temperature and the temperature has no drastic variation across the flow field, such as in aeroacoustics, the reference M , Re , and Pr will remain essentially constant over the whole field. Otherwise, the local variation of μ and κ with temperature will have to be determined from physical laws, such as the Sutherland law or the power law. In the present formulation, the path taken is to specify the reference M , Re , and Pr . If, in addition, μ and κ are temperature dependent, their relations with temperature also have to be defined. Otherwise, the local τ_{ij} and q_j as given by Eqs. (24) and (26), respectively, could not be evaluated properly. This requirement is no different from that required in solving the continuum N-S equations for flows where large gradients of ρ and/or T exist. As a result, all short comings of the continuum N-S equations for shock structure simulations [Brenner [32,33]; Greenshields and Reese [34]] would also show up in the current LBM solutions.

Solutions for Q'_j and P'_{ij} : Solving Eq. (27) with appropriate boundary conditions is one of many ways to determine Q'_j . Since Fu, et al. [28] have shown that there is no loss of generality in their attempt to recover the Euler equations exactly from the BGK-type modelled BE by assuming $Q'_j = 0$ to be valid; therefore, a trivial solution given by $Q'_j = 0$ can be adopted also as an alternative. Their modelled BE thus derived has been applied to simulate aeroacoustics problems, and excellent agreement was obtained between the LBM solutions of the modelled BE and those derived analytically or calculated from the Euler equations using DNS.

Provided Eq. (27) is satisfied, the macroscopic energy in Eq. (3) will remain unchanged no matter how Q'_j is constructed. Thus, the setting $Q'_j = 0$ is a simple assumption that gives rise to a correct recovery of the N-S equations. An alternative assumption can be made by invoking a Fourier heat conduction model, such as

$$Q'_j = \frac{1}{\text{Pr}_p} \frac{\partial T}{\partial x_j} \quad (28)$$

For particle-particle collision where Pr_p is its Prandtl number. This assumption might not be appropriate, because together with Eq. (27) it will impose an additional constraint $\partial^2 T / \partial x_j^2 = 0$ on the temperature behavior, which is not physical. An alternative way is to rewrite Eq. (23) in either one of the following two forms:

Delete Q'_j (i.e. setting $Q'_j = 0$ because it is actually redundant, and further note the absence of Q'_j in the lattice formulation (see Section 4, "Lattice f^{eq} and LBM Simulation")).

Writing $\int \frac{D_T + D_R}{D} \xi_j \frac{|\xi|^2}{2} f^{eq} d\xi = u_j(p + \rho e_i) + Q'_j$ and setting $Q'_j = q_j + u_k \tau_{kj}$, then

Eq. (27) is not required.

For the present formulation, a simple assumption of $Q'_j = 0$ can be invoked. Either one of these forms will allow the N-S equations to be recovered exactly. However, whether these conjectures are valid for the prediction of shock structures for diatomic gas will be examined later.

Having determined Q'_j , the next step is to solve for P'_{ij} subject to Eq. (25). The procedure to derive a solution for P'_{ij} in the Euler equations case has been fully outlined in Fu, et al. [28]. In the present case, it is anticipated that, because of the presence of τ_{ij} and q_j in Eqs. (22) and (23), respectively, the derived f^{eq} will be different from that given in Fu, et al. [28] for the Euler equations case. However, this is unlikely to affect the derivation for P'_{ij} . Therefore, the same procedure used to derive P'_{ij} will be followed with only a brief description given below (for details refer to [30]).

For 3-D flows in Cartesian coordinates, three partial differential equations can be written down for the elements of P'_{ij} . According to Eq. (22), P'_{ij} is symmetric. Even then, there are six unknowns in the three equations derived from Eq. (25). In order to have a close set of equations, three more equations are required. It should be noted that the trace of Eq. (22) together with $p = \rho\theta$ and Eq. (18) gives

$$\sum_1^D P'_i = \frac{D - (D_T + D_R)}{D_T + D_R} \rho |u|^2 - \sum_1^D \tau_i \tag{29}$$

A fourth equation for an element of P'_{ij} for $I \neq j$ can be obtained by differentiating the elemental equations of Eq. (25) with respect to x, y , and z , and making use of Eq. (29) after summing up the separate elemental equations to give

$$\begin{aligned} \frac{\partial^3}{\partial x \partial y \partial z} \left[\frac{D - (D_T + D_R)}{D_T + D_R} \rho |u|^2 - \sum_1^D \tau_i \right] + \frac{\partial}{\partial z} \left(\frac{\partial^2}{\partial x^2} + \frac{\partial^2}{\partial y^2} \right) P'_1 \\ + \frac{\partial}{\partial y} \left(\frac{\partial^2}{\partial x^2} + \frac{\partial^2}{\partial z^2} \right) P'_2 + \frac{\partial}{\partial x} \left(\frac{\partial^2}{\partial y^2} + \frac{\partial^2}{\partial z^2} \right) P'_3 = 0 \end{aligned} \tag{30}$$

Two more equations are required to form a close set for the determination of P'_{ij} . It should be noted that for the 2-D case, Eq. (30) is reduced to a second-order equation for P'_{12} . This suggests that the following isotropic assumption can be made for the 3-D case, such that

$$\frac{\partial^2}{\partial x \partial y} \left[\frac{D - (D_T + D_R)}{3(D_T + D_R)} \rho |u|^2 - \frac{1}{3} \sum_1^D \tau_i \right] + \left(\frac{\partial^2}{\partial x^2} + \frac{\partial^2}{\partial y^2} \right) P'_1 = 0 \tag{31a}$$

$$\frac{\partial^2}{\partial x \partial z} \left[\frac{D - (D_T + D_R)}{3(D_T + D_R)} \rho |u|^2 - \frac{1}{3} \sum_1^D \tau_i \right] + \left(\frac{\partial^2}{\partial x^2} + \frac{\partial^2}{\partial z^2} \right) P'_2 = 0 \tag{31b}$$

Taking the derivative of Eq. (31a) with respect to z and that of Eq. (31b) with respect to y and substituting them into Eq. (30) gives an equation for P'_{12} , or

$$\frac{\partial^3}{\partial x \partial y \partial z} \left[\frac{D - (D_T + D_R)}{3(D_T + D_R)} \rho |u|^2 - \frac{1}{3} \sum_1^D \tau_i \right] + \frac{\partial}{\partial x} \left(\frac{\partial^2}{\partial y^2} + \frac{\partial^2}{\partial z^2} \right) P'_3 = 0 \tag{32}$$

Consequently, three independent equations for P'_{ij} with $i \neq j$ are obtained. This choice of equations is not unique; presumably, the isotropic assumption can be made for any two-elemental combination of P'_{ij} with $i \neq j$. These three equations are of the Poisson type because of the presence of the cross-derivative term which is known. One possible solution set for P'_{ij} can now be written for an infinite domain R^D ($-\infty < x_i < \infty$) as

$$P'_j = - \int \sum_{k \neq i}^D \frac{\partial P'_k}{\partial x_k} dx_i \quad \text{for } i = j \tag{33a}$$

$$P'_j = \frac{1}{2\pi} \int \int_{-\infty}^{\infty} f(x'_i, x'_j) h \frac{1}{\sqrt{(x_i - x'_i)^2 + (x_j - x'_j)^2}} dx'_i dx'_j \quad \text{for } i \neq j \tag{33b}$$

Where $f(x'_i, x'_j) = \frac{D - (D_T + D_R)}{D_0(D_T + D_R)} \frac{\partial^2 \rho |u|^2}{\partial x'_i \partial x'_j} - \frac{1}{D_0} \sum_1^D \tau_i$ (33c)

With $D_0 = 1$ for 2-D flow and $D_0 = 3$ for 3-D flow, respectively.

Determination of f^{eq} : The solution of P'_{ij} depends on a

knowledge of ρ and $\rho \mathbf{u}$ which can be evaluated from Eqs. (13) and (14) once f^{eq} for diatomic gas is known. For monatomic gas, f^{eq} is given by the Maxwellian distribution function alone, as pointed out by Brenner [32-33]. The objective here is to find a modified f^{eq} for diatomic gas that could satisfy the constraints given by Eqs. (13) - (15), P'_{ij} , and Q'_j . The solution for P'_{ij} is given in Eqs. (33). That leaves f^{eq} to be determined. Fu, et al. [28] determined f^{eq} with guidance from previous analytical work [2,3,5,7]. It starts out by assuming

$$f^{eq} = \exp[A_o + A_i \xi_i + B_{mn} \xi_m \xi_n] \tag{34a}$$

Then factoring the Maxwellian term out of Eq. (34a), and the manipulation is followed by expanding the exponential function in terms of ξ_i to give

$$f^{eq} = \exp(-\eta |\xi_k - b_k|^2) [1 + A'_o + A'_i \xi_i + B'_{mn} \xi_m \xi_n + \dots] \tag{34b}$$

$$\begin{aligned} f^{eq} = \alpha_o \exp\left[-\eta \sum_{k=1}^D (\xi_k - b_k)^2\right] + \sum_{i=1}^D \alpha_i \xi_i \exp[-\eta |\xi|^2] + \sum_{m,n=1}^D \beta_{mn} \xi_m \xi_n \exp[-\eta |\xi|^2] \\ + \sum_{j=1}^D a_j \xi_j |\xi|^2 \exp[-\eta |\xi|^2] + \dots \end{aligned} \tag{34c}$$

Where α_o is a scalar, α_j , a_j , and b_i are vectors, β_{mn} is a second-order tensor, and η is a parameter to be determined. In the present formulation, it is found that the first few orders of the approximation from the general anisotropic Gaussian form is sufficient to define f^{eq} for all cases tested. The first term on the right-hand side of Eq. (34c) is the Maxwellian distribution function, while the following three terms are the first and second moments of the particle velocity. These additional terms, therefore, could be interpreted as a first attempt to partially model the nonlinear behavior resulting from particle-particle collisions due to particle dynamics alone and could not account for particle dynamics due to thermal effect. If the thermal effect were also to be accounted for, most likely another term involving q_i and/or e has to be added to Eq. (34c). Equation (34c) differs from conventionally known forms of f^{eq} proposed by other researchers. The presence of these three additional terms in Eq. (34) is sufficient to allow aeroacoustics disturbances and shock capturing to be resolved accurately [28, 32, 33]. In other words, the proposed modeling of particle-particle collisions in Eq. (34c) could correctly account for the effect of aerodynamic and acoustic interaction, flows with shocks, contact discontinuities, and expansion waves. It remains to be seen whether this same f^{eq} , but possibly with different α_o , α_j , a_j , b_i , and β_{mn} , is suitable for incompressible and compressible viscous flows.

The equations for α_o , α_j , a_j , b_i and β_{mn} can be derived from Eqs. (13) - (15), (22) and (23). The results are:

$$\rho = \left(\alpha_o + \sum_m^D \frac{\beta_{mm}}{2\eta} \right) \sqrt{\frac{\pi}{\eta}}^D \tag{35a}$$

$$\rho u_j = \left[\alpha_o b_j + \frac{\alpha_j}{2\eta} + \frac{(D+2)a_j}{4\eta^2} \right] \sqrt{\frac{\pi}{\eta}}^D \tag{35b}$$

$$\frac{2D}{D_T + D_R} \left(\rho e + \frac{1}{2} \rho |\mathbf{u}|^2 \right) = \frac{\rho D}{2\eta} + \sum_k^D \alpha_0 b_k^2 \sqrt{\frac{\pi^D}{\eta}} + \sum_m^D \frac{\beta_m}{2\eta^2} \sqrt{\frac{\pi^D}{\eta}} \quad (35c)$$

$$\rho u_i u_j + p \delta_{ij} + \tau_j + P'_j = \frac{\rho \delta_j}{2\eta} + \alpha_0 b_j b_j \sqrt{\frac{\pi^D}{\eta}} + \frac{\beta_j + \beta_j}{4\eta^2} \sqrt{\frac{\pi^D}{\eta}} \quad (35d)$$

$$\left(\frac{D}{2} + \frac{D}{D_T + D_R} \right) \rho u_j + \frac{D}{D_T + D_R} \frac{1}{2} \rho |\mathbf{u}|^2 u_j + \frac{D}{D_T + D_R} \left(q_j + \sum_k^D u_k \tau_k \right) = \left(1 + \frac{D}{2} \right) \frac{\rho u_j}{2\eta} + \frac{\alpha_0 b_j}{2} \sum_k^D b_k^2 \sqrt{\frac{\pi^D}{\eta}} + \frac{a_j}{8\eta^2} (D+2) \sqrt{\frac{\pi^D}{\eta}} \quad (35e)$$

From Eq. (35d), it is obvious that η could be determined by setting $p = \rho/2\eta$ as in the inviscid flow case. Since the state equation for diatomic gas is given by $p = \rho\theta$, η is evaluated to be $\eta = 1/2\theta$. The coefficients α_0 , α_j , a_j , b_j and β_{mn} can then be determined as

$$\alpha_0 = \frac{\rho}{\sqrt{2\pi\theta^D}} - \frac{D - (D_T + D_R)}{(D_T + D_R)\theta\sqrt{2\pi\theta^D}} \frac{1}{2} \rho |\mathbf{u}|^2 \quad (36a)$$

$$\alpha_j = \frac{1}{\theta} \left[\frac{\rho u_j}{\sqrt{2\pi\theta^D}} - \alpha_0 b_j - (D+2)\theta^2 a_j \right] \quad (36b)$$

$$a_j = \frac{1}{(D+2)\theta^3\sqrt{2\pi\theta^D}} \left[u_j p \left\{ \frac{D - (D_T + D_R)}{(D_T + D_R)} \right\} - \frac{b_j}{2} \rho |\mathbf{u}|^2 + \frac{D}{D_T + D_R} u_j \frac{1}{2} \rho |\mathbf{u}|^2 + \frac{D}{D_T + D_R} \left(q_j + \sum_k^D u_k \tau_k \right) \right] \quad (36c)$$

$$b_j = \frac{\pm u_j}{\sqrt{1 - \frac{D - (D_T + D_R)}{(D_T + D_R)\theta} \frac{1}{2} |\mathbf{u}|^2}} \quad (36d)$$

$$\beta_{ij} = \frac{\tau_{ij} + P'_{ij}}{2\theta^2\sqrt{2\pi\theta^D}} \quad (36e)$$

These coefficients are valid for both 2-D and 3-D flows and have no undefined constants. Also, it can be seen that the Maxwellian distribution function and the original BGK model can be correctly recovered for the case of “monatomic gas and inviscid flow”. However, the present formulation is not limited by these restrictions.

Thus deduced, an f^{eq} valid for diatomic gas is obtained and is given by Eq. (34c). In this expression, the first-order terms give rise to the N-S equations. To show that this is indeed the case, the procedure and method used to carry out this derivation are described in Section 4 below.

Lattice f^{eq} and LBM Simulation

It is necessary to write down the velocity space discretized form of Eq. (1). Since 1-D and 2-D flows are considered in the present paper; therefore, as an example, only the lattice counterpart of Eq. (1) in a 2-D domain is given. The 3-D counterpart can be similarly written by following the same procedure. The velocity space discretized form of Eq. (1) is given by

$$\frac{\partial f_\alpha}{\partial t} + \xi_\alpha \cdot \nabla_x f_\alpha = -\frac{1}{\tau Kn} (f_\alpha - f_\alpha^{eq}) \quad (37)$$

Where α is the index for the lattice velocity. In previous attempts on aeroacoustics and shock capturing, a D2Q9 lattice model was found to be sufficient for accurate resolution of the problems considered. However, certain problems might require a finer lattice. Therefore, a D2Q13 model is chosen for the lattice f_α^{eq} and is presented below. The reduction to a D2Q9 model is simple and will not be repeated. For a D2Q13 model, the lattice velocity is given by

$$\xi_0 = 0, \quad \alpha = 0 \quad (38a)$$

$$\xi_\alpha = \sigma \{ \cos[\pi(\alpha-1)/4], \sin[\pi(\alpha-1)/4] \}, \quad \alpha = 1, 3, 5, 7 \quad (38b)$$

$$\xi_\alpha = \sqrt{2}\sigma \{ \cos[\pi(\alpha-1)/4], \sin[\pi(\alpha-1)/4] \}, \quad \alpha = 2, 4, 6, 8 \quad (38c)$$

$$\xi_\alpha = 2\sigma \{ \cos[\pi(\alpha-1)/2], \sin[\pi(\alpha-1)/2] \}, \quad \alpha = 9, 10, 11, 12 \quad (38d)$$

Where σ is a parameter to be determined.

Just as in the case of the recovery of the Euler equations, as detailed in Fu, et al. [28] and So, et. al. [30], a polynomial series in ξ up to second order is assumed for the discretized form of f_α^{eq} , or

$$f_\alpha^{eq} = A_\alpha + \xi_{\alpha x} A x_\alpha + \xi_{\alpha y} A y_\alpha + \xi_{\alpha x}^2 B x x_\alpha + \xi_{\alpha y}^2 B y y_\alpha + \xi_{\alpha x} \xi_{\alpha y} B x y_\alpha \quad (39)$$

Here, the indices x and y are used to denote the stream and cross-stream direction in a 2-D flow, and the coefficients A_α , $A x_\alpha$, $B x x_\alpha$, etc., could be scalars, vectors, or tensors. In particular, this proposed lattice f^{eq} attempts to include the particle-particle collision effect of the additional terms in Eq. (34) into Eq. (39). However, it does not attempt to explicitly include the effect due to thermal heating of the particles. Its validity and appropriateness for aeroacoustics simulation and shock capturing have been demonstrated by Fu, et al. [28] and So, et al. [29] respectively, and by So, et al. [27] in a review of the development of a new LBM to treat a wide range of viscous incompressible and compressible flows of monatomic gas. In order to accomplish the present objective, therefore, it is necessary to further demonstrate that Eq. (39) is equally valid for LBM simulations of viscous incompressible and viscous compressible flow of diatomic gas with and without shocks.

The constraints, Eqs. (13) – (15), (22), and (23), used to recover the N-S equations in the continuous form are used to evaluate the coefficients in Eq. (39). For 2-D flows, the results are (with $N = 12$ for a D2Q13 model and $N = 8$ for a D2Q9 model):

$$\sum_{\alpha=0}^N f_\alpha^{eq} = \rho \quad (40a)$$

$$\sum_{\alpha=0}^N f_\alpha^{eq} \xi_{\alpha x} = \rho u \quad (40b)$$

$$\sum_{\alpha=0}^N f_\alpha^{eq} \xi_{\alpha y} = \rho v \quad (40c)$$

$$\sum_{\alpha=0}^N f_{\alpha}^{eq} (\xi_{\alpha x}^2 + \xi_{\alpha y}^2) = \frac{4}{D_T + D_R} \left(\rho e + \frac{1}{2} \rho |u|^2 \right) \tag{40d}$$

$$\sum_{\alpha=0}^N f_{\alpha}^{eq} \xi_{\alpha x}^2 = \rho u^2 + p + \tau_{xx} + P'_{xx} \tag{40e}$$

$$\sum_{\alpha=0}^N f_{\alpha}^{eq} \xi_{\alpha y}^2 = \rho v^2 + p + \tau_{yy} + P'_{yy} \tag{40f}$$

$$\sum_{\alpha=0}^N f_{\alpha}^{eq} \xi_{\alpha x} \xi_{\alpha y} = \rho uv + \tau_{xy} + P'_{xy} \tag{40g}$$

$$\sum_{\alpha=0}^N f_{\alpha}^{eq} (\xi_{\alpha x}^2 + \xi_{\alpha y}^2) \xi_{\alpha x} = \frac{4}{D_T + D_R} \left[u \left(\rho e + p + \frac{1}{2} \rho |u|^2 \right) + u \tau_{xx} + v \tau_{xy} + q_x \right] \tag{40h}$$

$$\sum_{\alpha=0}^N f_{\alpha}^{eq} (\xi_{\alpha x}^2 + \xi_{\alpha y}^2) \xi_{\alpha y} = \frac{4}{D_T + D_R} \left[v \left(\rho e + p + \frac{1}{2} \rho |u|^2 \right) + u \tau_{xy} + v \tau_{yy} + q_y \right] \tag{40i}$$

Where u and v are the velocity components along the x - and y -direction, respectively, and the elements of P'_{ij} are to be determined. These elements are obtained by solving the following three equations, which are given by Eqs. (25) and (29). For 2-D flows, they can be simplified to

$$\frac{\partial P'_x}{\partial x} + \frac{\partial P'_y}{\partial y} = 0 \tag{41a}$$

$$\frac{\partial P'_x}{\partial x} + \frac{\partial P'_y}{\partial y} = 0 \tag{41b}$$

$$\tau_x + \tau_y + P'_x + P'_y = \frac{2 - (D_T + D_R)}{D_T + D_R} \rho |u|^2 \tag{41c}$$

Of the nine equations, only eight are independent because one is a duplicate of the kinetic energy equation. These equations are used to determine $A_{\alpha}, Ax_{\alpha}, Bxx_{\alpha}$, etc. If the coefficients having the same “energy shell” of the lattice velocities are assumed to be the same, the number of unknowns resulting from the coefficients $A_{\alpha}, Ax_{\alpha}, Bxx_{\alpha}$, etc., are 19 in a D2Q13 lattice model. Since the number of constraints available for the determination of these coefficients is 8, there is certain flexibility, and reasonable assumptions can be made to facilitate the solution of the equations. As a first attempt, eleven coefficients out of the nineteen are assumed zero. Details of this derivation are given in Fu, et al. [28] and So, et al. [30]. The results are summarized here as:

$$A_0 = \rho - \frac{2p}{\sigma^2} - (\gamma - 1) \frac{\rho |u|^2}{\sigma^2}, \quad A_1 = A_2 = A_3 = 0 \tag{42a}$$

$$Ax_1 = \frac{2\rho u}{3\sigma^2} - \frac{1}{3} \frac{\gamma pu}{\sigma^4} - (\gamma - 1) \frac{1}{6} \frac{\rho |u|^2 u}{\sigma^4} - (\gamma - 1) \frac{q_x + u\tau_x + v\tau_y}{3\sigma^4}, \quad Ax_2 = 0 \tag{42b}$$

$$Ax_3 = -\frac{1}{24} \frac{\rho u}{\sigma^2} + \frac{1}{12} \frac{\gamma pu}{\sigma^4} + (\gamma - 1) \frac{1}{24} \frac{\rho |u|^2 u}{\sigma^4} + (\gamma - 1) \frac{q_x + u\tau_x + v\tau_y}{12\sigma^4} \tag{42c}$$

$$Ay_1 = \frac{2\rho v}{3\sigma^2} - \frac{1}{3} \frac{\gamma pv}{\sigma^4} - (\gamma - 1) \frac{1}{6} \frac{\rho |u|^2 v}{\sigma^4} - (\gamma - 1) \frac{q_y + u\tau_x + v\tau_y}{3\sigma^4}, \quad Ay_2 = 0 \tag{42d}$$

$$Ay_3 = -\frac{1}{24} \frac{\rho v}{\sigma^2} + \frac{1}{12} \frac{\gamma pv}{\sigma^4} + (\gamma - 1) \frac{1}{24} \frac{\rho |u|^2 v}{\sigma^4} + (\gamma - 1) \frac{q_y + u\tau_x + v\tau_y}{12\sigma^4} \tag{42e}$$

$$Bxx_1 = \frac{1}{2\sigma^4} (p + \rho u^2 + \tau_{xx} + P'_{xx}), \quad Bxx_2 = Bxx_3 = 0 \tag{42f}$$

$$Byy_1 = \frac{1}{2\sigma^4} (p + \rho v^2 + \tau_{yy} + P'_{yy}), \quad Byy_2 = Byy_3 = 0 \tag{42g}$$

$$Bxy_2 = \frac{1}{4\sigma^4} (\rho uv + \tau_{xy} + P'_{xy}), \quad Bxy_1 = Bxy_3 = 0 \tag{42h}$$

It should be noted that the solution thus obtained is not unique. However, there are no undefined constants, except σ , which satisfies the following restriction,

$$\min(|\xi_{\alpha}|^2) \sum_{\alpha=0}^N f_{\alpha}^{eq} \leq \frac{4}{D_T + D_R} \left(\rho e + \frac{1}{2} \rho |u|^2 \right) \leq \max(|\xi_{\alpha}|^2) \sum_{\alpha=0}^N f_{\alpha}^{eq} \tag{43}$$

Simplification for viscous flows with $M \ll 1$: For incompressible viscous flows, the expressions for the continuous and lattice f^{eq} function could be further reduced to simpler forms because ρ is constant, the equation of state and the energy equation are satisfied automatically, and the only unknowns are u and p . The normalization could be modified (e.g., changing c_r to U_r); however, it is not crucial in the derivation of the f^{eq} functions outlined below.

According to Eq. (36c), the coefficient a_j is essentially related to the energy of the fluid flow, while the coefficient β_{ij} in Eq.(36e) is a function of τ_{ij} and P'_{ij} . With the energy equation automatically satisfied, this suggests that the term in Eq. (34c) associated with a_j might not play an important role in the case of incompressible viscous flows. The term associated with the coefficient α_j , i.e. Eq. (36b), is then reduced to one very similar to Eq. (36a). Hence, it could be absorbed into Eq. (36a). Consequently, the form for f^{eq} could be reduced to two terms given by

$$f^{eq} = \alpha_0 \exp \left[-\eta \sum_{k=1}^D (\xi_k - b_k)^2 \right] + \sum_{m,n=1}^D \beta_{mn} \xi_m \xi_n \exp \left[-\eta |\xi|^2 \right] \tag{44}$$

Using the constraints given by Eqs. (13), (14), and (22), the following expressions for $\rho, \rho u_j, p$ and P'_{ij} are obtained:

$$\rho = \left(\alpha_0 + \sum_m^D \frac{\beta_{mm}}{2\eta} \right) \sqrt{\frac{\pi}{\eta}} \tag{45a}$$

$$\rho u_j = \alpha_0 b_j \sqrt{\frac{\pi}{\eta}} \tag{45b}$$

$$\rho u_i u_j + p \delta_{ij} + \tau_{ij} + P'_{ij} = \frac{\rho \delta_{ij}}{2\eta} + \alpha_0 b_i b_j \sqrt{\frac{\pi}{\eta}} + \frac{\beta_{ij} + \beta_{ji}}{4\eta^2} \sqrt{\frac{\pi}{\eta}} \tag{45c}$$

Again, η can be determined to be $\eta = \rho/2p$, and the coefficients $\alpha_0 b_j$ and β_{ij} are found to be given by

$$\alpha_0 = \rho / (2p\pi / \rho)^{D/2} \tag{46a}$$

$$b_j = u_j \tag{46b}$$

$$\beta_{ij} = \frac{\rho^2}{2p^2} \left[\frac{\tau_{ij} + P'_{ij}}{(2p\pi / \rho)^{D/2}} \right] \tag{46c}$$

Where P'_{ij} can be deduced from Eq. (25) and the result is:

$$\sum_i P'_i = -\sum_i \tau_i \tag{46d}$$

Equation (46d) shows that P'_{ij} and τ_{ij} appear together; therefore, there is no loss of generality to assume that P'_{ij} could be absorbed into τ_{ij} (even though it might be more appropriate to construct P'_{ij} as before; however, later calculation shows that this is not at all necessary). In view of this realization, the lattice counterpart of the constraints for the discretized form of f^{eq}_α can be written as

$$\sum_{\alpha=0}^N f^{eq}_\alpha = \rho \tag{47a}$$

$$\sum_{\alpha=0}^N f^{eq}_\alpha \xi_{\alpha x} = \rho u \tag{47b}$$

$$\sum_{\alpha=0}^N f^{eq}_\alpha \xi_{\alpha y} = \rho v \tag{47c}$$

$$\sum_{\alpha=0}^N f^{eq}_\alpha \xi_{\alpha x}^2 = \rho u^2 + p + \tau_{xx} \tag{47d}$$

$$\sum_{\alpha=0}^N f^{eq}_\alpha \xi_{\alpha y}^2 = \rho v^2 + p + \tau_{yy} \tag{47e}$$

$$\sum_{\alpha=0}^N f^{eq}_\alpha \xi_{\alpha x} \xi_{\alpha y} = \rho uv + \tau_{xy} \tag{47f}$$

A polynomial expansion of Eq. (44) would lead to a discretized form of f^{eq}_α very similar to Eq. (39). Following the procedure for a D2Q9 model, one possible set of solutions is

$$A_0 = \rho - \frac{2p}{\sigma^2} - \frac{\rho|\mathbf{u}|^2}{\sigma^2} - \frac{\tau_{xx} + \tau_{yy}}{\sigma^2}, \quad A_1 = A_2 = 0 \tag{48a}$$

$$Ax_1 = \frac{\rho u}{2\sigma^2}, \quad Ax_2 = 0 \tag{48b}$$

$$Ay_1 = \frac{\rho v}{2\sigma^2}, \quad Ay_2 = 0 \tag{48c}$$

$$Bxx_1 = \frac{1}{2\sigma^4}(p + \rho u^2 + \tau_{xx}), \quad Bxx_2 = 0 \tag{48d}$$

$$Byy_1 = \frac{1}{2\sigma^4}(p + \rho v^2 + \tau_{yy}), \quad Byy_2 = 0 \tag{48e}$$

$$Bxy_1 = 0, \quad Bxy_2 = \frac{1}{4\sigma^4}(\rho uv + \tau_{xy}) \tag{48f}$$

The elimination of P'_{ij} in the lattice form of f^{eq} suggests that, by choosing other forms of f^{eq} rather than those given by Eqs. (44a-f), one might arrive at the choice of $P'_{ij}=0$ in the case of the continuous form for f^{eq} too. Therefore, there is no need to construct P'_{ij} for the case of incompressible viscous flows. Even then, the form of f^{eq} is different from the original BGK model and includes a term that could be interpreted as partially accounting for the physics of particle-particle collisions; thus, providing a way to extend the LBM to account for the effect of particle-particle collisions resulting from diatomic gas flow.

Alternative LBM simulation: The discrete Boltzmann equation, i.e. Eq. (37), can be viewed as a system of inhomogeneous hyperbolic equations. Therefore, any standard finite difference scheme can be used to solve it. Traditional LBM is only second-order accurate in both spatial and temporal dimensions, thus, it is not suitable for direct aeroacoustics simulation (DAS). In the present investigation, the terms on the right-hand side of Eq. (37) are evaluated locally at every time step. A second-order Runge-Kutta time marching scheme is used to calculate the time-dependent term in Eq. (37), while the second term on the left-hand side of Eq. (37) is estimated using a sixth-order finite difference scheme proposed by Lele [31]. Details of the present numerical scheme used to solve the discretized modelled BE have been thoroughly discussed in So, et al. [30]. The relaxation time τ in Eq. (37) could be specified as follows. In the present formulation, τ and Kn always appear together as τKn in Eq. (37), thus implying that τ and Kn need not be specified separately. Since τ is of $O(1)$ and Kn is assumed to be very small; of the order of 10^{-7} according to Chapman and Cowling [1], the term τKn should be much smaller than 1 when compared to other terms in Eq. (37). In the present calculation, $\Delta t = \tau Kn = 10^{-5}$ is chosen because this is sufficient to give results identical to those obtained with DNS. Furthermore, numerical instability was not encountered in all calculations carried out, even without high-order filters.

Since the absorbing boundary condition suggested by Kam, et al. [35] was found to give reliable and accurate results compared to those obtained from DNS simulations using a dimensionless absorbing region of 1, it is also invoked in the present study. As for the damping coefficient, its choice varies from problem to problem; therefore, it will be specified when the specific problem is discussed. In the present study, a D2Q9 model is used, similar to all calculations carried out by Li, et al. [17,36] and Kam, et al. [35]. The boundary conditions for solid walls are specified as $u_{n+1} = v_{n+1} = 0$ at the walls (no slip), $p_{n+1} = p_n$, $\rho_{n+1} = \rho_n$, where subscript $n+1$ is the boundary point and n is the immediate point next to the boundary. From these specifications, the boundary conditions for f and f^{eq} can be determined. As for the boundary conditions for P'_{ij} , they are discussed in the next section.

Alternatively, Eq. (37) can be solved by any other numerical method; but it is not easy to set a proper boundary condition for f_α . This is because it is sometimes difficult to find a corresponding f_α for any physical boundary condition expressed in macroscopic quantities. Therefore, devising a suitable numerical method to solve Eq. (37) is important. It is proposed to adopt a splitting method such that the equation is solved in two stages; traditionally, they are viewed as the free streaming stage and the collision stage. For the free streaming stage, the homogenous hyperbolic equation is solved first,

$$\frac{\partial f_\alpha}{\partial t} + \xi_\alpha \cdot \nabla_x f_\alpha = 0 \tag{49a}$$

A second-order Runge-Kutta time marching scheme is used to calculate the time-dependent term, while the second term on the left-hand side of Eq. (49a) is estimated using a sixth-order finite difference scheme proposed by Lele [31]. Next, for the collision stage, the results obtained in the first stage act as an initial condition for the differential equation below,

$$\frac{\partial f_\alpha}{\partial t} = -\frac{1}{\tau Kn} (f_\alpha - f_\alpha^{eq}) \quad (49b)$$

Which is discretized by the Euler method with the choice $\Delta t = \tau Kn$. Thus,

$$\frac{f_\alpha(\bar{x}, t + \Delta t) - f_\alpha(\bar{x}, t)}{\Delta t} = -\frac{1}{\tau} (f_\alpha(\bar{x}, t) - f_\alpha^{eq}(\bar{x}, t)) \quad (49c)$$

$$\Rightarrow f_\alpha(\bar{x}, t + \Delta t) = f_\alpha^{eq}(\bar{x}, t)$$

With this clarification, the numerical procedure can now be summarized as follows:

- i. Given a distribution function f_α at time t , after the free streaming stage, an intermediate value for f_α' is obtained.
- ii. Using this f_α' and Eq. (40), the macroscopic quantities (ρ , u , v , p) can be determined.
- iii. Boundary condition set at the macroscopic level is adopted here as is common for any finite difference method.
- iv. Using the macroscopic quantities and through the expression given in Eq. (39), $(f_\alpha')^{eq}$ can be determined.
- v. Adopting Eq. (49c), the collision stage is then completed by exactly setting the new f_α as the equilibrium distribution function $(f_\alpha')^{eq}$ in (iv). For each set of macroscopic quantities, it will map to a unique equilibrium distribution function, and for each set of equilibrium distribution functions, it will map to a unique set of macroscopic quantities, so the macroscopic quantities obtained are in fact, the values at time $t + \Delta t$.

This procedure indirectly shows that the accuracy of this scheme is of $O(\Delta t)$ because both the splitting method and the Euler method are only first-order accurate in time. In fact, recovery of the N-S equation also has an error $O(Kn) = O(\Delta t) = 1e^{-5}$. Even then, accuracy up to order 10^{-7} compared with DNS results can still be realized.

Solution of P'_{ij} in the LBM scheme: The individual elements of P'_{ij} are given by solving the following equations,

$$\frac{\partial P'_{ij}}{\partial x_j} = 0 \quad (50a)$$

$$P'_{kk} = A \quad (50b)$$

Where $A = \left[\frac{(D - D_T - D_R)}{(D_T + D_R)} \right] \rho |u|^2 + \sum \tau_{kk}$ for the N-S equations, while the viscous stress term τ_{kk} in A would be identically zero for the Euler equations. All the macroscopic quantities (ρ, u, p), including the physical boundary, are

contained in A . In the 2-D case considered here, Eqs. (50a, b) reduce to

$$\frac{\partial P'_{xx}}{\partial x} + \frac{\partial P'_{xy}}{\partial y} = 0 \quad (51a)$$

$$\frac{\partial P'_{xy}}{\partial x} + \frac{\partial P'_{yy}}{\partial y} = 0 \quad (51b)$$

$$P'_{xx} + P'_{yy} = A \quad (51c)$$

For the present analysis, it is assumed that all functions are sufficiently smooth for their derivatives to exist. A Poisson equation can be derived from Eqs. (51a-c) through differentiation and invoking Eq. (51c); the result is

$$\frac{\partial^2 A}{\partial x \partial y} + \left(\frac{\partial^2}{\partial x^2} + \frac{\partial^2}{\partial y^2} \right) P'_{xy} = 0 \quad (52)$$

On the other hand, taking the derivative of Eq. (51a) with respect to x , and that of Eq. (51b) with respect to y , and then subtracting, the following is obtained:

$$\frac{\partial^2 P'_{xx}}{\partial x^2} - \frac{\partial^2 P'_{yy}}{\partial y^2} = 0 \quad (53)$$

After using Eq. (51c), another Poisson equation is deduced, i.e.

$$-\frac{\partial^2 A}{\partial y^2} + \left(\frac{\partial^2}{\partial x^2} + \frac{\partial^2}{\partial y^2} \right) P'_{xx} = 0 \quad (54)$$

Similarly, an equation for P'_{yy} also can be obtained. Solving Eqs. (51a, b, c) and Eq. (53) with suitable boundary conditions and using Eq. (51c), P'_{xy} , P'_{yy} and P'_{xx} can be determined. The boundary conditions for these equations are given below.

A finite rectangular domain with four boundaries, namely top, bottom, left, and right, represented by $y = H$, $y = 0$, $x = 0$, and $x = L$, respectively, is assumed. In solving Eq. (52), the Neumann condition is assumed for the top and bottom boundaries, i.e.,

$$\frac{\partial P'_{xy}}{\partial y} = 0 \text{ at } y = 0, H \quad (55)$$

While the Dirichlet condition is assumed for the left and right boundaries, or,

$$P'_{xy} = k_{1L} \text{ at } x = 0, \quad P'_{xy} = k_{1R} \text{ at } x = L \quad (56)$$

Where k_{1L} and k_{1R} are constants. On the other hand, in solving Eq. (54), the Dirichlet condition is invoked for the top and bottom boundaries,

$$P'_{xx} = k_{2B} \text{ at } y = 0, \quad P'_{xx} = k_{2T} \text{ at } y = H \quad (57)$$

Where k_{2B} and k_{2T} are constants, and the Neumann condition is prescribed for the left and right boundaries, or,

$$\frac{\partial P'_{xx}}{\partial x} = 0 \text{ at } x = 0, L \quad (58)$$

Compatibility: Eq. (56) implies that on the left and right boundaries the y -derivative of P'_{xy} vanishes. Similarly, the condition given by Eq. (57) implies that on the top and bottom boundaries the x -derivative of P'_{xx} vanishes. Therefore, combining Eq. (55) and Eq. (58) ensures that Eq. (51a) is satisfied on all four boundaries. Taking the derivative of Eq. (51a) with respect to x , and using Eq. (54), the following equation is obtained,

$$\frac{\partial^2 P'_{xy}}{\partial x \partial y} + \frac{\partial^2 P'_{yy}}{\partial^2 y} = 0 \quad (59a)$$

Similarly, taking the derivative of Eq. (51a) with respect to y , and using Eq. (52),

$$\frac{\partial^2 P'_{xy}}{\partial^2 x} + \frac{\partial^2 P'_{yy}}{\partial x \partial y} = 0 \quad (59b)$$

Eq. (59b) is obtained. This means that, on the boundary, Eqs. (59a) and (59b) must be satisfied simultaneously. The only choice is

$$\frac{\partial P'_{xy}}{\partial x} + \frac{\partial P'_{yy}}{\partial y} = k \quad (59c)$$

Where k is an arbitrary constant. Therefore, Eq. (59c) holds on all four boundaries, which is a weaker condition compared to Eq. (51b).

It can be shown that using the above-proposed boundary conditions, solving Eqs. (52), (54), and (51c) is equivalent to solving a weaker system of Eqs. (51a), (59c) and (51c) in the whole domain. Taking the derivative of Eq. (52) with respect to y , that of Eq. (54) with respect to x , and then summing up gives

$$\left(\frac{\partial^2}{\partial x^2} + \frac{\partial^2}{\partial y^2} \right) \left(\frac{\partial P'_{xx}}{\partial x} + \frac{\partial P'_{xy}}{\partial y} \right) = 0 \quad (60)$$

Which is the Laplacian of the LHS of Eq. (51a). Since Eq. (51a) is satisfied along the boundary, then due to Eq. (60), Eq. (51a) is satisfied in the whole domain ($\because \nabla^2 u = 0$ & $u|_{bdy} = 0 \Leftrightarrow u \equiv 0$). With the help of Eq. (51c) and using a similar technique as that given above gives

$$\left(\frac{\partial^2}{\partial x^2} + \frac{\partial^2}{\partial y^2} \right) \left(\frac{\partial P'_{xy}}{\partial x} + \frac{\partial P'_{yy}}{\partial y} \right) = 0 \quad (61)$$

Similarly, Eq. (59c) is satisfied along the boundary; therefore, due to Eq. (61), Eq. (59c) is satisfied in the whole domain (by the maximum principle for the Laplace equation).

The weaker system (represented by Eqs. (51a), (59c), and (51c)) is different from the original system given by Eqs. (50a-c). This implies that the constant ' k ' in Eq. (59c) might not be zero. If the weaker system were to return to the original system, k has to be zero. In order to find the condition under which this is true, double integrate Eq. (59c) along x and y to give

$$\begin{aligned} & \int_0^H \int_0^L \left[\frac{\partial P'_{xy}}{\partial x} - \frac{\partial P'_{xx}}{\partial y} + \frac{\partial A}{\partial y} = k \right] dx dy \\ & \Rightarrow \int_0^H \int_0^L \frac{\partial P'_{xy}}{\partial x} dx dy - \int_0^H \int_0^L \frac{\partial P'_{xx}}{\partial y} dy dx + \int_0^H \int_0^L \frac{\partial A}{\partial y} dy dx = kLH \\ & \Rightarrow \int_0^H P'_{xy}|_{x=L} - P'_{xy}|_{x=0} dy - \int_0^L P'_{xx}|_{y=H} - P'_{xx}|_{y=0} dx + \int_0^L A|_{y=H} - A|_{y=0} dx = kLH \\ & \Rightarrow (k_{1R} - k_{1L})H - (k_{2T} - k_{2B})L + \int_0^L A|_{y=H} - A|_{y=0} dx = kLH \end{aligned} \quad (62)$$

Therefore, Eq. (61) shows that in order to achieve $k = 0$, the simplest conditions are:

$$\begin{aligned} k_{1R} &= k_{1L} = k_{2B} = 0 \\ k_{2T} &= \frac{1}{L} \int_0^L A|_{y=H} - A|_{y=0} dx \end{aligned} \quad (63)$$

Validation of the Improved LBM for flows with $M \ll 1$

The recovered N-S equations and the associated boundary conditions for the modelled BE and P'_i are verified for their validity and extent against aeroacoustics problems. Three cases are considered. These problems are selected to test the ability of the modelled BE to reflect the effect of time and Re correctly, then the effectiveness of the proposed no-slip boundary conditions for the modelled BE, and finally the ability of the modelled BE to replicate the vorticity-acoustics, and entropy-acoustics interactions correctly. The three problems chosen for aeroacoustics are: (i) propagation of a circular pulse in an infinite medium, (ii) propagation of a circular pulse in an enclosure bounded by four walls, and (iii) interactions of a vorticity, an entropy, and an acoustic pulse in a moving stream. Whenever possible, the improved LBM simulations are validated against analytical results or against DNS of Eqs. (1)–(6) using a fourth-order Runge-Kutta time marching scheme for the time-dependent term and a sixth-order numerical scheme adopted by Lele [31] for the convective terms. No-slip boundary conditions are invoked at solid boundaries, while the absorbing boundary condition adopted by Leung, et al. [37] is used in all computational boundaries other than solid walls. Unless otherwise specified, all cases investigated using the improved LBM, σ is estimated from Eq. (43). All other constants in the improved LBM are either derived analytically or known; therefore, arbitrary constants are absent. As such, the improved LBM solution should be identical to the DNS result of the same problem.

The error norms between the improved LBM and analytical or numerical solution of the N-S equations (DNS and/or DAS) of a macroscopic variable \mathbf{b} are expressed in terms of the L_q integral norm as

$$\|L_q(\mathbf{b})\| = \left[\frac{1}{N} \sum_{j=1}^N |\mathbf{b}_{LBM,j} - \mathbf{b}_{DNS,j}|^q \right]^{\frac{1}{q}} \quad (64a)$$

For any integer q , and its maximum

$$\|L_\infty(\mathbf{b})\| = \max_j |\mathbf{b}_{LBM,j} - \mathbf{b}_{DNS,j}| \quad (64b)$$

Thus defined, the calculated error norms of p , u , and ρ will be tabulated for comparisons for the different cases studied.

Aeroacoustics and their simulation results: Direct aeroacoustics simulation is taxing on the numerical scheme as well as on the modelled BE. The reason is due to the disparity of scales [16,35] and the numerical accuracy required if the aeroacoustics scales were to be resolved correctly [28]. If the improved LBM could accurately replicate benchmark aeroacoustics problems correctly, including resolving the nonlinear interactions between flow and acoustics and the effect of Re on these interactions, then the improved LBM can claim to be a viable and valid numerical method for this class of problems. Therefore, it is important to test the improved LBM on the classical aeroacoustics problems first. The following classical aeroacoustics problems have been identified. They are Case (i) a circular pulse in an infinite medium, Case (ii) a circular pulse in an enclosure, and Case (iii) three pulses in a uniform stream. These results are presented and discussed separately below.

Case (i) – circular pulse in an infinite medium:

A circular pressure pulse located at $(x, y) = (0, 0)$ has an initial distribution given by

$$\rho = \rho_\infty, \quad u = 0, \quad v = 0, \quad p = p_\infty + \varepsilon \exp\left(-h \cdot 2 \times \frac{x^2 + y^2}{0.2^2}\right) \quad (65)$$

Where $\rho_\infty = 1$, $\rho_\infty = 1/\gamma$, and ε chosen to be $\varepsilon = 1 \times 10^{-4}$ is simulated using the improved LBM and performing a DNS of the N-S equations. Other numerical conditions specified are: $\Delta t = 0.00001$, $\Delta x = \Delta y = 0.05$, computational domain is bounded by $-3.5 \leq x (y) \leq 3.5$ with one unit of buffer region (i.e. the actual domain is given by $-2.5 \leq x, (y) \leq 2.5$), $Pr_\infty = 0.71$ and $Re_\infty = 10, 100, 1000$ and infinite (inviscid). From this point on, the subscript ∞ is used to denote the reference condition. The numerical settings for DNS are given by $\Delta x = \Delta y = 0.05$, $\Delta t = 0.001$. Therefore, the ratio $\Delta x/\Delta t = \Delta y/\Delta t = 5 \times 10^3$ for the improved LBM is 100 times larger than that used in the DNS simulation.

The results of this simulation are shown in So, et al. [30] and Figures 1-4. Figures 1 and 2 display the contour plots of $p - \rho_\infty$ and $u - u_\infty$, respectively. Figure 3 shows the contour plots of p'_i , while Figures 4a and 4b give the distribution plots of the velocity components. All these plots are drawn from computation results at $t = 1$. In addition, the inviscid result together with those given by $Re_\infty = 10, 100$, and 1000 are plotted in the same figure for comparison. In Figures 1 and 2, the upper half displays the improved LBM results while the lower half shows the DNS results. It can be seen that the $p - \rho_\infty$ and $u - u_\infty$ contours in the two halves are essentially identical. The largest error norm is of the order of 10^{-9} while the smallest is of 10^{-10} . This is true for all Re_∞ cases examined [30]. They

show that the present 6th-order finite-difference scheme used by So, et al. [27] to resolve the modelled Boltzmann equation and the N-S equations are quite suitable for aeroacoustics problems.

The values of the P'_i components (Figure 3) are small, but they are still two orders of magnitude greater than the error norms; therefore, they are significant and cannot be neglected. The role of viscosity is to diffuse the wave and this role is clearly illustrated in the panels of $Re_\infty = 100$ (left side of figure) and panels of $Re_\infty = 10$ (right side of figure) in Figures 1-3. As far as the circular pulse is concerned, $Re_\infty = 1000$ is sufficiently inviscid already. This is further substantiated by the distribution plots shown for the velocity components u and v (Figure 4). The $Re_\infty = 1000$ solution is essentially identical to the inviscid result. From these results, it can be seen that as Re_∞ decreases, the diffusion of the wave becomes more and more pronounced; this is reflected in a substantial reduction of the waves' amplitude. Together, these results suggest that, for all practical purposes, it is quite appropriate to use it to treat high Re wave propagation in the solution of the Euler equations.

Case (ii) – circular pulse in an enclosure: The propagation of a circular pressure pulse located at $(x, y) = (-1, 0)$ inside an enclosure with initial conditions given by

$$\rho = \rho_\infty, \quad u = u_\infty, \quad v = v_\infty, \quad p = p_\infty + \varepsilon \exp(-\ln 2((x+1)^2 + y^2)/0.2^2) \quad (66)$$

is investigated. For this example, $u_\infty = v_\infty = 0$, $\rho_\infty = 1$, $p_\infty = 1/\gamma$, $\varepsilon = 10^{-4}$ are chosen together with $M_\infty = 1$, $Re_\infty = 1000$, $Pr_\infty = 0.71$, and $\gamma = 1.4$. Again, the numerical settings are given by $\Delta x = \Delta y = 0.05$, while $\Delta t = 0.001$ is selected for DNS, and $\Delta t = 0.00001$ for LBM. The effectiveness of the proposed wall boundary condition for f can be shown by the contour maps of $(p - p_\infty)$ and $(u - u_\infty)$ in So et al. [30]. All three components of p'_i in a 2-D flow are shown in Figure 5. The error norms between the improved LBM and DNS results are tabulated in So, et al. [30]; the smallest error norm is of order 10^{-10} while the largest is of order 10^{-8} , consistent with those given in Case (i). Clearly, these results show that the wall boundary condition proposed for f is valid; consequently, the error norms between the two solutions are extremely small.

Case (iii) – three pulses in a uniform stream:

The three-pulses are a pressure pulse, a vorticity pulse, and an entropy pulse propagating in a uniform mean flow u_∞ . Only the pressure pulse is propagating with speed c , the entropy pulse and the vortex pulse move with u_∞ . The initial conditions specified in Tam and Webb [38] are:

$$\rho = \rho_\infty + \varepsilon_1 e^a + \varepsilon_2 e^b, \quad p = p_\infty + \varepsilon_1 e^a \quad (67a)$$

$$u = u_\infty + \varepsilon_2 y e^b, \quad v = v_\infty - \varepsilon_2 (x - 1) e^b \quad (67b)$$

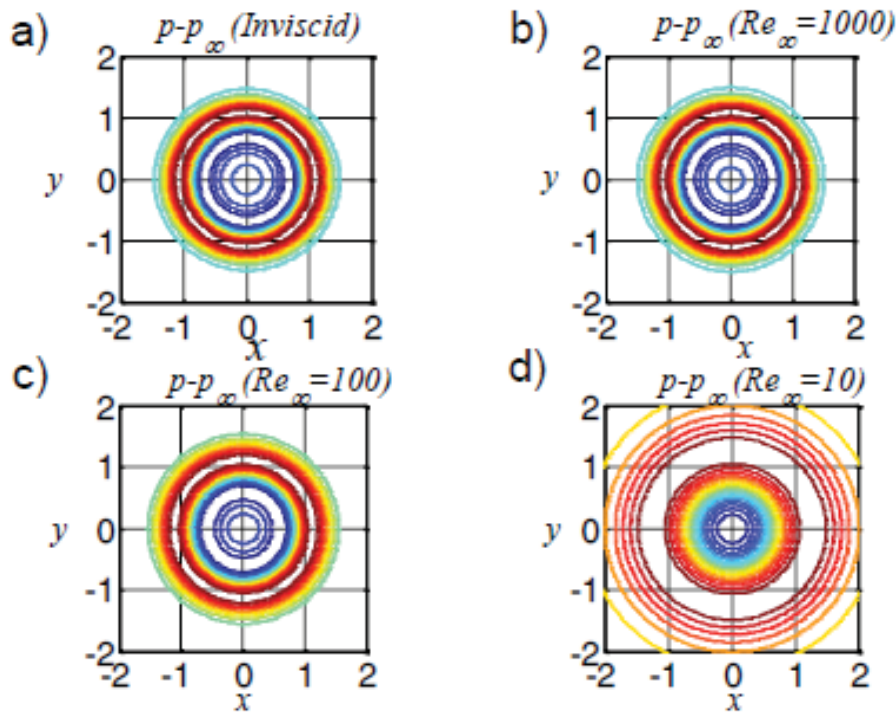


Figure 1: Contour plots (with 16 contour lines) of $p - p_\infty$ at $t = 1$ for four Re_∞ : there are 16 contour lines with (max, min) given by $(1.4594e-005, -9.1947e-006)$ for inviscid flow; $(1.3889e-005, -8.8471e-006)$ for $Re_\infty = 1000$; $(9.7796e-006, -6.8992e-006)$ for $Re_\infty = 100$; and $(2.8246e-006, -4.5021e-006)$ for $Re_\infty = 10$ in each plot. The upper half is the improved LBM solution and the lower half is the DNS result.

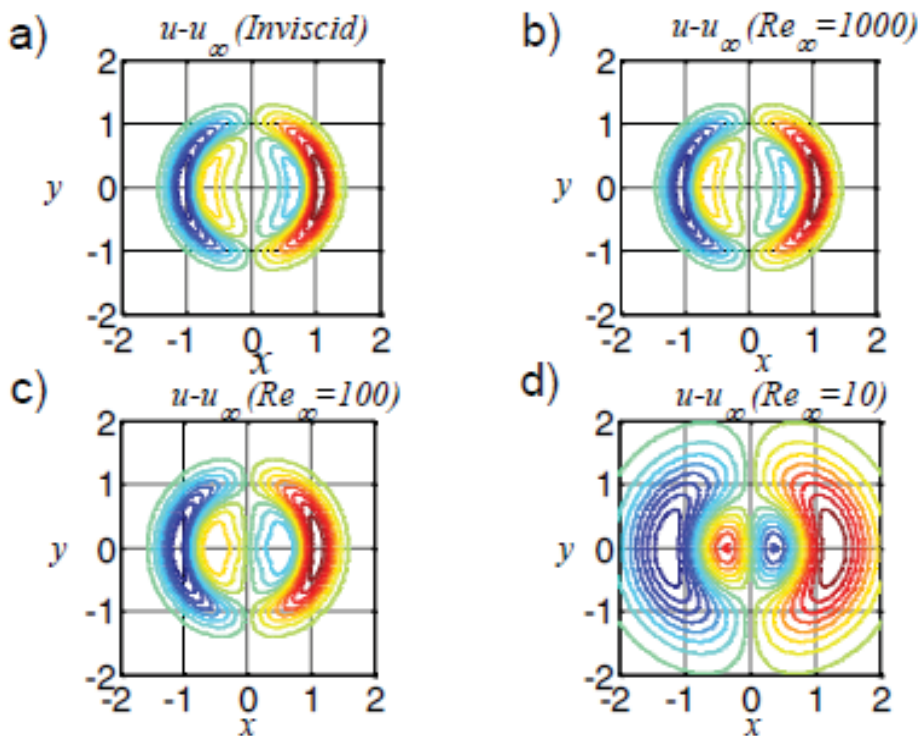


Figure 2: Contour plots (with 16 contour lines) of $u - u_\infty$ at $t = 1$ for four Re_∞ : there are 16 contour lines with (max, min) given by $(1.5713e-005, -1.5713e-005)$ for inviscid flow; $(1.5042e-005, -1.5042e-005)$ for $Re_\infty = 1000$; $(1.0899e-005, -1.0899e-005)$ for $Re_\infty = 100$; and $(3.1526e-006, -3.1526e-006)$ for $Re_\infty = 10$ in each plot. The upper half is the improved LBM solution and the lower half is the DNS result.

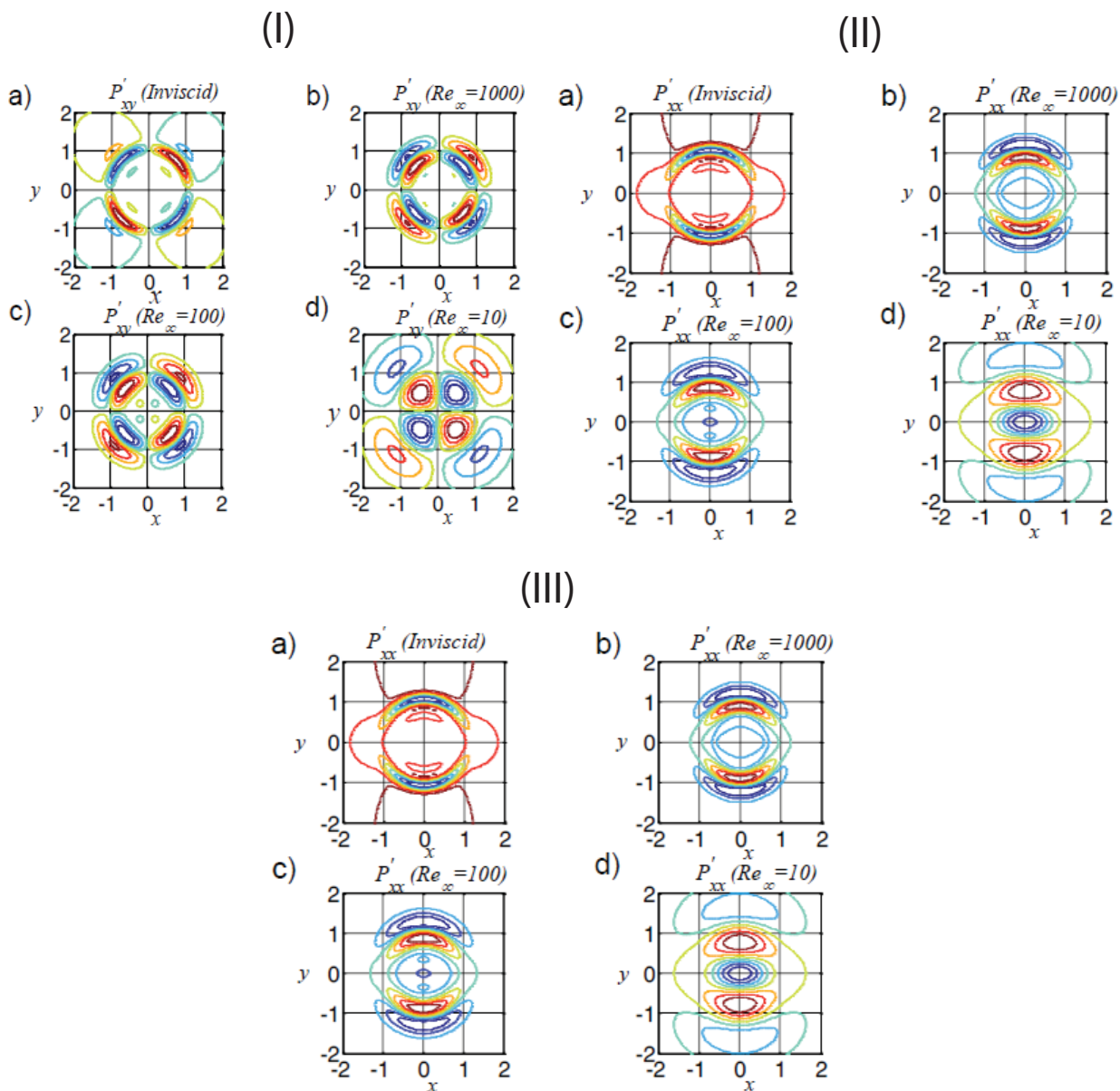


Figure 3: Contour plots (with 8 contour lines) of p'_i for four different Re :
(I) -- Plots for P'_{xy} the (max, min) for inviscid flow is (5.8990e-011, -5.8980e-011), for $Re = 1000$ is (2.7677e-008, -2.7685e-008), for $Re_{\infty} = 100$ is (1.5651e-007, -1.5655e-007), and for $Re_{\infty} = 10$ is (3.1678e-007, -3.1682e-007).
(II) --- P'_{xx} the (max, min) for inviscid flow is (2.0625e-011, -1.3168e-010), for $Re_{\infty} = 1000$ is (5.9169e-008, -3.8018e-008), for $Re_{\infty} = 100$ is (3.3780e-007, -2.1940e-007), and for $Re_{\infty} = 10$ is (6.2764e-007, -5.8298e-007).
(III) --- P'_{yy} the (max, min) for inviscid flow is (2.0704e-011, -1.3177e-010), for $Re_{\infty} = 1000$ is (5.9184e-008, -3.7942e-008), for $Re_{\infty} = 100$ is (3.3789e-007, -2.1884e-007), and for $Re_{\infty} = 10$ is (6.2730e-007, -5.8425e-007).

$$a = -\ln 2 \left(\frac{(x+1)^2 + y^2}{0.2^2} \right), \quad b = -\ln 2 \left(\frac{(x-1)^2 + y^2}{0.4^2} \right) \quad (67c)$$

Where $\varepsilon_1 = 0.000$ and $\varepsilon_2 = 0.001$. The reference density, speed, and pressure are given by $\rho_{\infty} = 1, u_{\infty} = 0.9, v_{\infty} = 0, p_{\infty} = 1/\gamma$. Under the present formulation, u_{∞} is identical to M_{∞} . This problem has been treated by Fu, et al. [28] using the modelled BE to recover the Euler equations and they choose $u_{\infty} = M_{\infty} =$

0.9. Therefore, the present simulation will again specify $M_{\infty} = 0.9$ in addition to stipulating $Pr_{\infty} = 0.71$ and $Re_{\infty} = 10, 100,$ and 1000 plus the inviscid calculation.

The $(p - p_{\infty})$ and $(u - u_{\infty})$ contours are plotted in Figures 6 and 7, respectively, while those for P'_i are shown in Figure 8. All Re_{∞} cases calculated, including the inviscid case, are depicted in each figure. They illustrate the effect of Re on the propagation of the pressure pulse and its interaction with

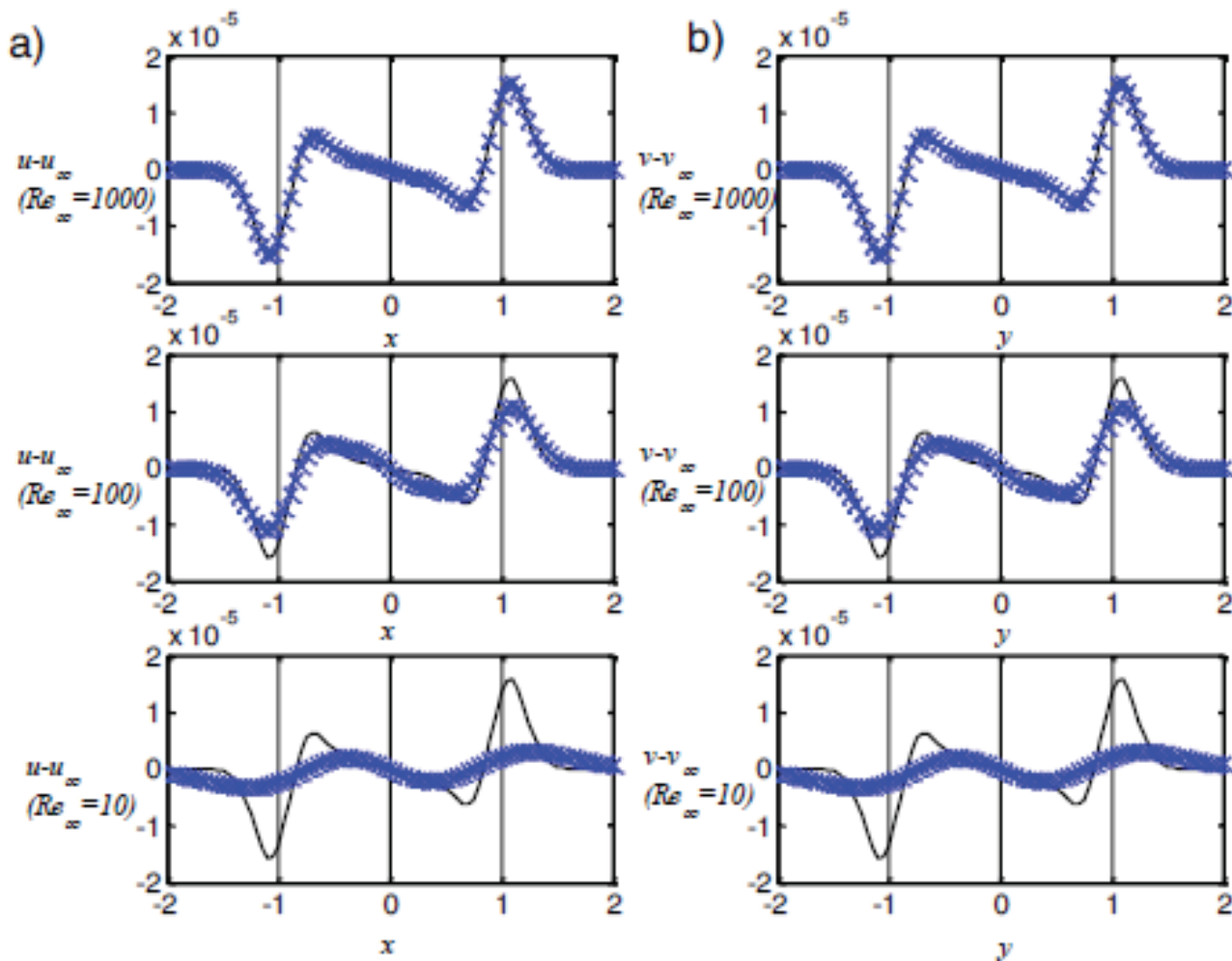


Figure 4: Distribution of u and v at $t = 1$ for different Re_∞ : (a) u along x -axis, b) v along y -axis. The black dash curve is the inviscid solution, the blue curve represents the DNS results, and the blue crosses represent the improved LBM results.

the entropy and vorticity pulse. It can be seen that as Re_∞ decreases, the pressure contours become more and more diffuse with similar behavior recorded for the components of P'_{ij} . Just as in Case (i), the magnitude of P'_{yy} is orders of magnitude larger than the other two components (Figure 8). Therefore, it plays a major role in the correct calculation of the interaction between the three pulses. All these results show that the improved LBM solutions are essentially identical to those given by DNS. Further evidence can be found in the calculated error norms tabulated in So, et al. [30]. The error norms have a low of 10^{-9} and a high of 10^{-7} . These values are at least one order better than those reported in Li et al. [17, 36] using the same 6th-order finite-difference scheme but solving a different modelled BE.

Validation of the improved LBM for flows with $M > 1$

The ability of the LBM to correctly simulate aeroacoustics, compressible flows with shocks, and shock structure has been thoroughly studied and reported in [29,30]. In the

shock structure problems, Argon and Nitrogen shocks at different M are attempted. The validity of the N-S equations to replicate shock structure is investigated together with remedies proposed by Brenner [32,33], and Greenshields and Reese [34]. It can be shown that the modelled BE, which can give an exact recovery of the N-S equations, suffers the same inadequacy as the N-S equations themselves; therefore, the remedies suggested by Brenner [32,33] can also be built into the analytically derived f^{eq} .

Shock structure simulation results: The objective of this section is to simulate the structure of a steady plane shock where the thickness is so thin that it challenges the validity of the continuum assumption. This is a 1-D boundary value problem. The governing equation is the 1-D steady N-S equation which in dimensionless form can be written as

$$\frac{\partial}{\partial x}(\rho u) = 0 \tag{68}$$

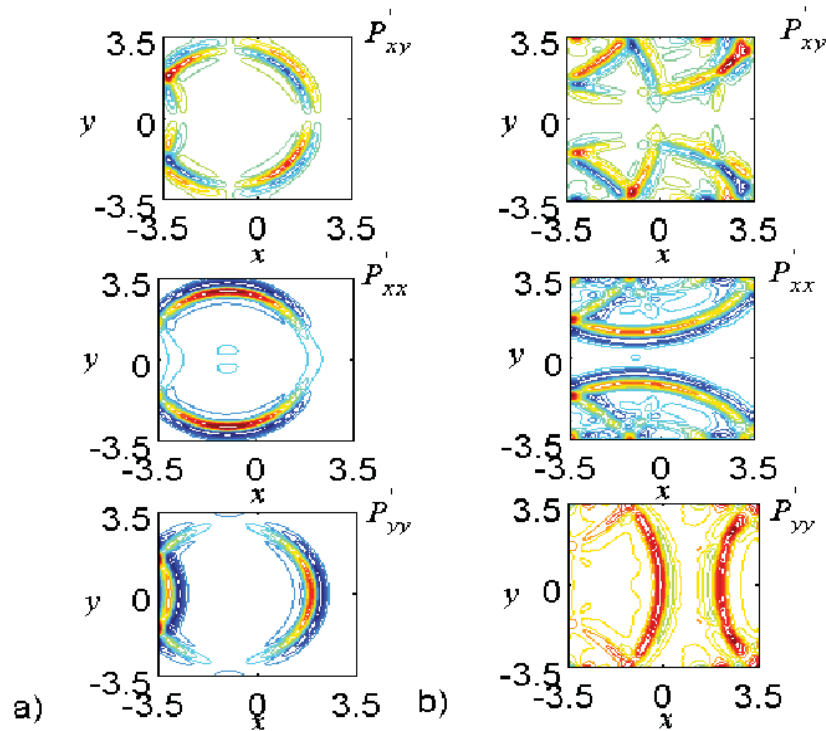


Figure 5: Contour map of the P'_{xy} , P'_{xx} and P'_{yy} fluctuation at (a) $t = 3.0$ and (b) $t = 6.0$. The lower half is the DNS solution; the upper half is the improved LBM simulation. There are 16 equally distributed contour lines in each plot, and the (max, min) values at $t = 3.0$ and $t = 6.0$ are (2.1881e-008, -2.1887e-008) for P'_{xy} , (3.2134e-008, -1.6665e-008) for P'_{xx} (3.9055e-008, -1.9992e-008) for P'_{yy} ; and (1.2511e-008, -1.2508e-008) for P'_{xy} , (2.5122e-008, -1.4689e-008) for P'_{xx} , (2.0682e-008, -4.1409e-008) for P'_{yy} , respectively.

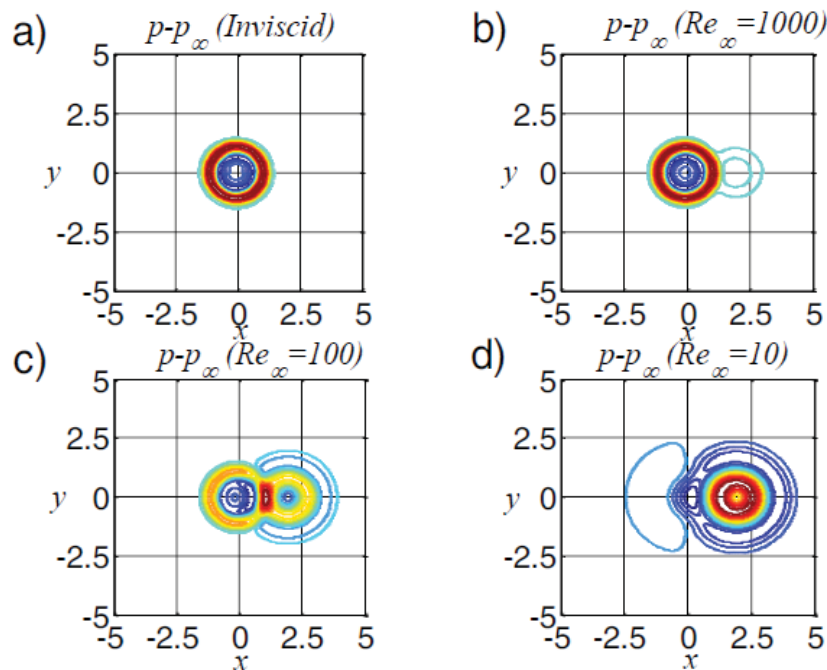


Figure 6: Contour plots of $p - p_{\infty}$ at $t = 1$ for four Re_{∞} : there are 16 contour lines with (max, min) given by (1.4619e-005, -9.6695e-006) for inviscid flow; (1.4809e-005, -9.3697e-006) for $Re_{\infty} = 1000$; (1.7862e-005, -1.0858e-005) for $Re_{\infty} = 100$; and (3.9522e-005, -1.6379e-005) for $Re_{\infty} = 10$ in each plot. The upper half is the improved LBM solution and the lower half is the DNS result.

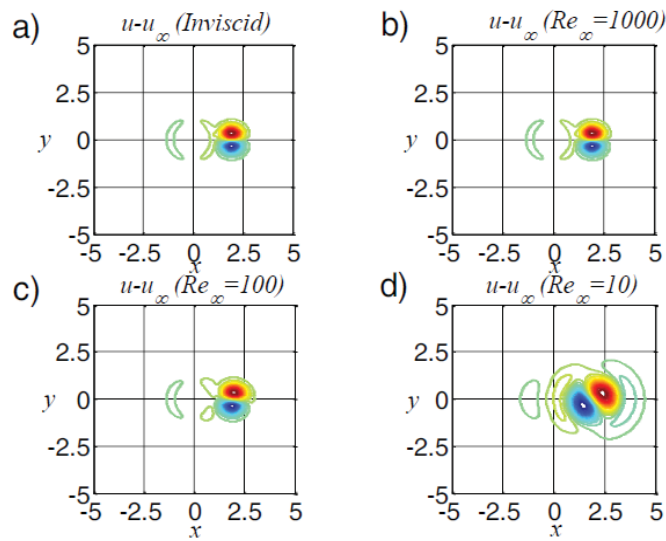


Figure 7: Contour plots of $u - u_\infty$ at $t = 1$ for four Re_∞ ; there are 16 contour lines with (max, min) given by $(2.0576e-004, -2.0582e-004)$ for inviscid flow; $(2.0105e-004, -2.0123e-004)$ for $Re_\infty = 1000$; $(1.6647e-004, -1.6663e-004)$ for $Re_\infty = 100$; and $(9.3840e-005, -9.1715e-005)$ for $Re_\infty = 10$ in each plot. The upper half is the improved LBM solution and the lower half is the DNS result.

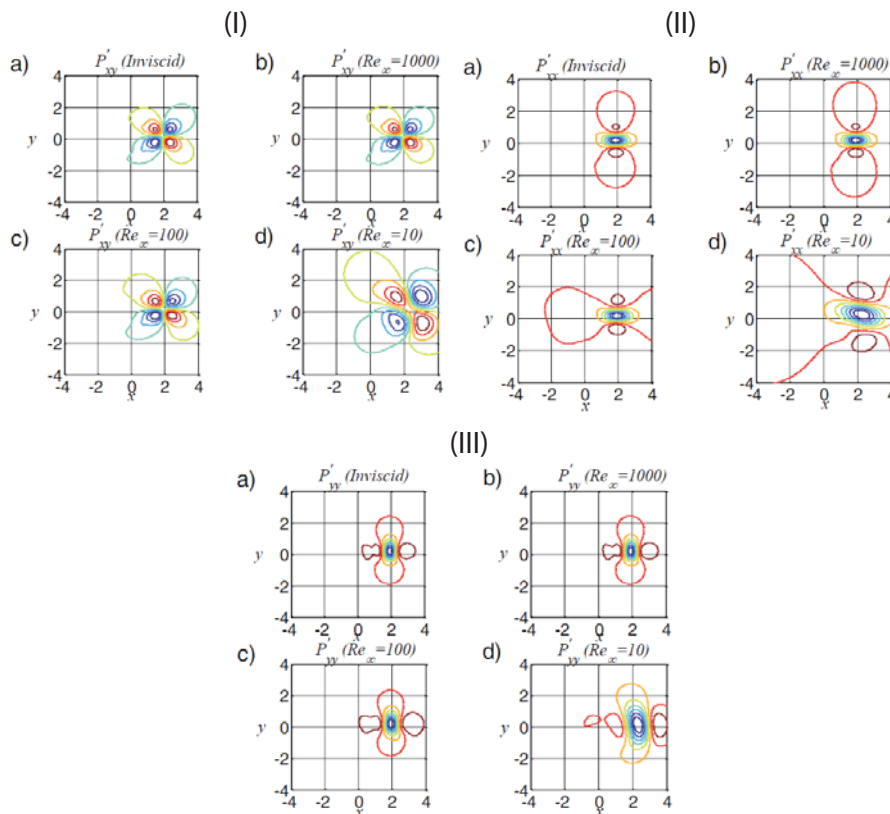


Figure 8: Contour plots (with 8 contour lines) of P'_y for four different Re :
(I) --- P'_y the (max, min) for inviscid flow is $(9.7981e-005, -9.6920e-005)$, for $Re_\infty = 1000$ is $(9.5376e-005, -9.4783e-005)$, for $Re_\infty = 100$ is $(7.6808e-005, -7.7825e-005)$, and for $Re_\infty = 10$ is $(3.7115e-005, -3.8695e-005)$.
(II) --- P'_xx the (max, min) for inviscid flow is $(9.9110e-005, -3.1951e-004)$, for $Re_\infty = 1000$ is $(9.3853e-005, -3.1522e-004)$, for $Re_\infty = 100$ is $(7.0335e-005, -2.6445e-004)$, and for $Re_\infty = 10$ is $(2.9201e-005, -1.0627e-004)$;
(III) --- P'_yy the (max, min) for inviscid flow is $(-0.4859, -0.4863)$, for $Re_\infty = 1000$ is $(-0.4859, -0.4863)$, for $Re_\infty = 100$ is $(-0.4860, -0.4862)$, and for $Re_\infty = 10$ is $(-0.4860, -0.4861)$.

$$\frac{\partial}{\partial x} \left[p + \rho u^2 - \frac{2\mu M}{\text{Re}} \frac{\partial u}{\partial x} - \frac{\lambda M}{\text{Re}} \frac{\partial u}{\partial x} \right] = 0 \quad (69)$$

$$\frac{\partial}{\partial x} \left[u \left(p + \rho e + \frac{1}{2} \rho u^2 \right) - \frac{\mu \gamma M}{\text{PrRe}} \frac{\partial e}{\partial x} - u \frac{2\mu M}{\text{Re}} \frac{\partial u}{\partial x} - u \frac{\lambda M}{\text{Re}} \frac{\partial u}{\partial x} \right] = 0 \quad (70)$$

Where λ is the second coefficient of viscosity. Asymptotically, the shock structure is bounded by two equilibrium states. The boundary condition is related by the Rankine-Huguenot condition, which can be specified as,

$$\frac{\rho_2}{\rho_1} = \frac{u_1}{u_2} = \frac{(\gamma+1)M_1^2}{2+(\gamma-1)M_1^2}, \quad \frac{p_2}{p_1} = 1 + \frac{2\gamma(M_1^2-1)}{\gamma+1} \quad (71)$$

Where subscript '1' and '2' represent the state ahead (upstream) and behind (downstream) the shock, respectively. The state ahead of the shock (state '1') is used as a reference. The characteristic length is chosen to be the mean free path, which is given by

$$L = \frac{16}{5\sqrt{\pi}} \frac{\hat{\mu}_1}{\hat{\rho}_1 \sqrt{2RT_1}} \quad (72)$$

Where the 'hat' is again used to denote dimensional quantities. Therefore, the reference Reynolds number $\text{Re}_\infty = \text{Re}$ is given by

$$\text{Re} = \frac{\rho_1 u_1 L}{\hat{\mu}_1} = \frac{16}{5\sqrt{2\pi/\gamma}} \frac{u_1}{\sqrt{\gamma RT_1}} = \frac{16}{5\sqrt{2\pi/\gamma}} M_1 \quad (73)$$

Since the shock is a steady one, the shock Mach number is the Mach number ahead of the shock, i.e., $M_\infty = M_1$. The power law is used to represent the variation of viscosity μ with temperature T ,

$$\mu = \frac{\hat{\mu}}{\hat{\mu}_1} = \left(\frac{\hat{T}}{\hat{T}_1} \right)^s = \left(\frac{p/\hat{p}}{p_1/\hat{p}_1} \right)^s = \left(\frac{p}{p_1} \frac{\rho_1}{\rho} \right)^s \quad (74)$$

Where exponent (s) is a constant equal to 0.816 and 0.756 for Argon and Nitrogen gas, respectively. A similar power law will also be assumed for the thermal conductivity κ [1]. For the second coefficient of viscosity, Stokes's hypothesis is adopted, i.e., $\lambda = -2\mu/3$, which is suitable for monatomic gas, but doubtful for polyatomic gas as pointed out by Gilbarg and Paolucci [39].

The solution of Eqs. (67) - (69) is obtained by solving their unsteady counterparts until a steady-state solution has been reached. The initial condition is given by

$$\rho = \begin{cases} \rho_1 \\ \rho_2 \end{cases}, \quad u = \begin{cases} u_1 \\ u_2 \end{cases}, \quad p = \begin{cases} p_1 & \text{for } x < 0 \\ p_2 & \text{for } x \geq 0 \end{cases} \quad (75)$$

A fixed boundary state denoted by subscript '1' at $x \rightarrow -\infty$ is set so that

$$\rho_1 = 1, \quad u_1 = M_1, \quad p_1 = 1/\gamma \quad (76)$$

While the boundary state '2' at $x \rightarrow +\infty$ is set according

to the Rankine-Huguenot condition given in Eq. (71). Data is presented in the form of a normalized value \tilde{A} , which is defined as

$$\tilde{A} = \frac{A - A_1}{A_2 - A_1} \quad (77)$$

Improved LBM simulation of shock structure: Three cases were demonstrated in So, et al. [30]; they are the Argon shocks at $M = 1.2$ and at $M = 1.55$ reported in Ohwada [40], and the Nitrogen shock at $M = 1.53$ reported in Alsmeyer [41]. The numerical simulations are given by the improved LBM and the solution of Eqs. (68) - (70) are compared with the DNS result of Ohwada [40] and the experimental measurements of Alsmeyer [41]. Since this is a 1-D shock, $P'_{xx} = P'_{yy} = 0$. Therefore, the only nonzero component in P'_j is P'_{yy} . Its distribution for each shock can be found in So, et al. [30]. Two observations can be made: the first is that the present numerical results, either obtained from the improved LBM or from solving Eqs. (68) - (70), are essentially identical; thus showing that the recovery of the N-S equations from the modelled BE is exact. However, these results do not quite agree with either the DNS result or the experimental measurements. The simulated results are symmetric about $x = 0$ while the DNS and experimental measurements show asymmetry to different degrees dependent on whether the gas is Argon or Nitrogen. The discrepancy between simulations and other data increases from Argon to Nitrogen shock as the asymmetry becomes more and more acute. The second observation is that the magnitude and behavior of P'_{yy} follows closely that of the shock profile. This indicates the importance of P'_{yy} in the improved LBM simulation. It could be speculated that if the contribution of P'_{yy} is absent, like in conventional LBM, the simulated shock structure would most likely be less correct. In order to understand these discrepancies, a close examination of the nature of shock structures is necessary. Through this examination, it is hoped that a remedy could be found to improve the present numerical simulations.

Physics of shock structure: Macroscopically, a shock wave appears as a discontinuity; however, this is not the case in the microscopic dimension. The calculation of the structure of a stationary shock often represents a challenge for models of rarefied gas flow, because Kn is no longer small; therefore, the continuum assumption is not quite valid. Thomas [42] argued for Becker's idea that only kinetic theory and BE, but not any continuum method, are capable of simulating shock structure correctly. Hence, solving the BE seems to be another viable approach for any shock structure problem. Following the kinetic theory and starting from the BE or a modelled BE, it could be expected that getting higher order terms in the Chapman-Enskog expansion could for example result in the Burnett equation, thus the likelihood of simulating shock structure properly. However, Wang-Chang, et al. [3]

showed that the Chapman-Enskog theory yields a series that converges so slowly that it is doubtful whether they have any validity unless $M \approx 1$ [2]. Furthermore, Mott-Smith [2] concluded that “the Chapman-Enskog theory is not applicable to strong shock.” Subsequently, Salwen, et al. [5] proposed a bimodal distribution for strong shock and extended the proposal by adding ‘correction terms’ to bring the method back into agreement with hydrodynamic theories for weak shock. In numerical simulation, Chu [43] employed a two reduced-functions approach. A discrete ordinate method was used to solve the governing equations by first removing the velocity space dependency from the distribution functions so that the BE could be solved in the phase space. However, the most commonly accepted solution method for the BE in the simulation of shock structure is the direct simulation Monte Carlo (DSMC) method of Bird [44]. This simulation is often used as a benchmark for testing new numerical schemes [45] or new kinetic models for rarefied flow [46,47].

Although the concept of a continuum might not be meaningful in shock structure simulation, researchers are not willing to give up the macroscopic approach; they proposed to modify the N-S equations to achieve an extended hydrodynamic model that might be suitable for rarefied gas. Gilbarg and Paolucci [39] explored the consequences and potentialities of continuum methods to simulate shock structure in detail. Weiss [48] showed by numerical calculation that extended hydrodynamic equations developed by the method of moment have restrictions related to M . Continuous shock structure only exists up to a critical M , e.g. no continuous shock beyond $M = 1.65$ exists by invoking Grad’s 13-moment theory. Recently, Brenner [32,33] proposed modifications to the N-S equations that are based on theoretical arguments. It is hypothesized that the velocity appearing in the velocity gradient term in Newton’s rheological law should be changed from the fluid’s mass-based velocity to its volume-based velocity. Since the proposal has supporting experimental evidence, discernible improvement for the shock structure is obtained if these new equations were solved rather than the N-S equations. Therefore, it is worth investigating the extension of the Brenner-Navier-Stokes model [33] to the improved LBM to see if the same improvements can be obtained, and this is the reason why such cases were calculated in So, et al. [30].

Brenner correction applied to the improved LBM: The normalized Brenner-N-S equations are given by the following:

$$\frac{\partial \rho}{\partial t} + \frac{\partial}{\partial x_j} (\rho u_j) = 0 \quad (78)$$

$$\frac{\partial (\rho u_i)}{\partial t} + \frac{\partial}{\partial x_j} [\rho \delta_{ij} + \rho u_i u_j - T_{ij}] = 0 \quad (79)$$

$$\frac{\partial}{\partial t} \left(\rho e + \frac{1}{2} \rho |u|^2 \right) + \frac{\partial}{\partial x_j} \quad (80)$$

$$\left[u_j \left(p + \rho e + \frac{1}{2} \rho |u|^2 \right) - u_k T_{jk} - \frac{\gamma M}{\text{Pr Re}} \frac{\partial e}{\partial x_j} - \frac{M}{\text{Pr}_2 \text{ Re}} \frac{\mu p}{\rho^2} \frac{\partial \rho}{\partial x_j} \right] = 0$$

Where the stress tensor T_{ij} (It should be noted that T without any subscripts is still used to denote temperature.) is modified by adding an additional term B_{ij} as given below

$$T_{ij} = \frac{\mu M}{\text{Re}} \left(\frac{\partial u_j}{\partial x_i} + \frac{\partial u_i}{\partial x_j} \right) + \frac{\lambda M}{\text{Re}} \frac{\partial u_k}{\partial x_k} \delta_{ij} + B_{ij} \quad (81)$$

$$B_{ij} = \left\langle \frac{2\mu M^2}{\text{Re}^2 \text{Pr}_2} \frac{\partial}{\partial x_i} \left(\frac{\mu}{\rho^2} \frac{\partial \rho}{\partial x_j} \right) \right\rangle$$

And the square bracket is defined as

$$\langle A \rangle \equiv A'' - (1/3) \text{tr}(A'') I, \quad A'' \equiv (A + A^T) / 2 \quad (82)$$

The parameter Pr_2 is defined as the ratio of the kinematic viscosity to the volume diffusivity coefficient by Brenner [32, 33]. As suggested by Greenshields and Reese [34], it should be greater than or equal to unity to avoid nonphysical behavior. For 1-D steady flow, the governing equations for shock problems are reduced to

$$\frac{\partial}{\partial x} (\rho u) = 0 \quad (83)$$

$$\frac{\partial}{\partial x} \left[p + \rho u^2 - \frac{2\mu M}{\text{Re}} \frac{\partial u}{\partial x} - \frac{\lambda M}{\text{Re}} \frac{\partial u}{\partial x} - \frac{4\mu M^2}{3\text{Re}^2 \text{Pr}_2} \frac{\partial}{\partial x} \left(\frac{\mu}{\rho^2} \frac{\partial \rho}{\partial x} \right) \right] = 0 \quad (84)$$

$$\frac{\partial}{\partial x} \left[u \left(p + \rho e + \frac{1}{2} \rho u^2 \right) - \frac{\mu \gamma M}{\text{Pr Re}} \frac{\partial e}{\partial x} - u \frac{2\mu M}{\text{Re}} \frac{\partial u}{\partial x} - u \frac{\lambda M}{\text{Re}} \frac{\partial u}{\partial x} - \frac{M}{\text{Pr}_2 \text{ Re}} \frac{\mu p}{\rho^2} \frac{\partial \rho}{\partial x} \right] = 0 \quad (85)$$

In these equations, Power law is again used to represent the variation of μ and κ , while temperature T and λ are related to μ by the Stokes relation.

The Brenner-Navier-Stokes model [32, 33] is given by Eqs. (83) – (85). Similarly, the improved LBM could be modified by requiring the modelled BE to recover Eqs. (78) – (80) with T_{ij} given by Eq. (81). The procedure is identical to that given above for the recovery of the N-S equations and the lattice counterpart can again be deduced by following the procedure outlined in Section 3. Therefore, the derivation details are omitted here. The simulation results for the Argon shock at $M = 1.55$ and the Nitrogen shock at $M = 1.53$ can be found in So, et al. [30]. In all the simulations, power law variation with temperature has been assumed for μ and κ . For the Argon shock, Brenner’s correction is sufficient to bring the simulation results to agree with the measurements. In other words, for monatomic gas, Brenner’s correction is sufficient to model the collision behavior of the gas particles to allow an

extension of the small Kn assumption to replicate the shock structure up to $M = 1.55$. The same correction proves to be inadequate for a diatomic gas at about the same M . This shows that the extension of the continuum assumption to a high M flow of non-equilibrium compressible flow is not viable. The improved LBM results are identical to those given by the Brenner-Navier-Stokes model simulation. Since the improved LBM recovers the continuum N-S equations and its Brenner correction exactly, this failure is not surprising. The improved LBM is limited by the Chapman-Enskog expansion which is an expansion in terms of Kn . If the shock structure of diatomic gas were to be replicated correctly, the small Kn assumption invoked for the improved LBM has to be relaxed.

Conclusion

A way to correctly recover the Navier-Stokes equations for incompressible and compressible diatomic gas flows from a BGK-type modelled Boltzmann equation has been proposed and formulated by So, et al. [30]. This BGK-type modelled BE is based on a generalized equilibrium particle distribution function that is derived by considering moments of the particle distribution function. Thus formulated, the equilibrium particle distribution function has four terms; the leading term is a Maxwellian, while the other three terms are moments of the particle distribution function. The presence of these terms allows the rotational dynamic behaviour of the particles to be considered in the formulation of the improved LBM. A singular advantage of this approach is that it allows the N-S equations to be recovered from the first-order expansion of the distribution function. Thus, it is not restricted by the $M \ll 1$ assumption and is formulated for diatomic gas. The reason this assumption is not necessary is that second-order or higher-order expansion terms in the distribution function are not required. However, the present methodology cannot be used to recover the transport coefficients of the fluid because, in the process of recovering the N-S equation, one stipulation has to be made, i.e., the reference M , Re , Pr , have to be specified, much like in the non-dimensional N-S equations where these non-dimensional numbers are assumed to be known. This methodology is also valid and viable for the recovery of different fluid dynamic governing equations subject to the $Kn \ll 1$ assumption.

The improved BGK-type modelled BE is resolved to assume a velocity lattice at each grid point of a finite difference scheme used to solve the lattice equations numerically. For two-dimensional problems, only a nine-velocity-lattice model is required. Validations are carried out against benchmark aeroacoustics problems and one-dimensional structures of Argon and Nitrogen shocks. Excellent agreement between the improved LBM results and those obtained from direct numerical simulation (DNS) of the N-S equations has been achieved for all aeroacoustics problems investigated, including

acoustics wave propagation inside an enclosure, in an infinite medium, and interaction with entropy and vorticity waves.

In the shock structure problems attempted, it is found that the improved LBM solutions are in perfect agreement with those derived from DNS, but they are not in agreement with experimental measurements. The discrepancy for the Argon shock could be remedied through a modification made to the N-S equations suggested by Brenner [32, 33]. However, disagreement is still noticeable for Nitrogen shocks even after the modifications had been implemented. This could be traced to the inadequacy of the continuum assumption in both the N-S equations and in the modelled Boltzmann equation because, within the shock layer, Kn is not necessarily very small; this is especially true for diatomic gas shock. In view of this, there is a need to further improve the modelled Boltzmann equation so that it is valid over a wider range of Kn . Consequently, it can be said that the modelled Boltzmann equation suffers the same limitations as the N-S equations. Its only advantage is the solution of one scalar equation for aerodynamics problems ranging from incompressible to compressible flows with and without shocks; therefore, computational errors associated with numerically solving the N-S equations could be avoided.

Acknowledgements

Administrative and computer support provided by the Mechanical Engineering Department,

The Hong Kong Polytechnic University, Kowloon, HKSAR, PRC are gratefully acknowledged.

References

1. Chapman S, Cowling TG. The Mathematical Theory of Non-uniform Gases. Cambridge University Press; 1939. Chapter 12.
2. Mott-Smith HM. The solution of the Boltzmann equation for a shock wave. *Phys Rev.* 1951;82:885-892.
3. Wang-Chang CS, Uhlenbeck GE, deBoer J, editors. *Studies in Statistical Mechanics*. Wiley; 1964; 2.
4. Morse TF. Kinetic model for gases with internal degrees of freedom. *Phys Fluids.* 1964;7:159-169.
5. Salwen H, Grousch CE, Ziering S. Extension of the Mott-Smith method for a one-dimensional shock wave. *Phys Fluids.* 1964;7:180-189.
6. Holway LH. New statistical models for kinetic theory: methods of construction. *Phys Fluids.* 1966;9:1658-1673.
7. Bhatnagar PL, Gross EP, Krook M. A model for collision processes in gases: I. Small amplitude processes in charged and neutral one-component systems. *Phys Rev.* 1954;94:511-525.
8. Broadwell J. Study of rarefied shear flow by the discrete velocity method. *Phys Fluids.* 1964;7:1243.
9. Cao NS, Chen S, Jin S, Martinez D. Physical symmetry and lattice symmetry in the lattice Boltzmann method. *Phys Rev E.* 1997;55:R21-24.
10. Mei R, Shyy W. On the finite difference-based lattice Boltzmann method in curvilinear coordinates. *J Comput Phys.* 1998;143:426-448.
11. Wolf-Gladrow DA. *Lattice-Gas Cellular Automata and Lattice Boltzmann Models: An Introduction*. Springer Verlag; 2000. Chapter 5.

12. Alexander FJ, Chen S, Sterling JD. Lattice Boltzmann thermohydrodynamics. *Phys Rev E*. 1993;47:R2249-R2252.
13. McNamara GR, Alder B. Analysis of the lattice Boltzmann treatment of hydrodynamics. *Physica A*. 1993;194:218-228.
14. Hu S, Yan G, Shi W. A lattice Boltzmann model for compressible perfect gas. *Acta Mechanica Sinica (English Edition)*. 1997;13:218-226.
15. Kataoka T, Tsutahara M. Lattice Boltzmann model for the compressible Navier-Stokes equations with flexible specific-heat ratio. *Phys Rev E Stat Nonlin Soft Matter Phys*. 2004 Mar;69(3 Pt 2):035701. doi: 10.1103/PhysRevE.69.035701. Epub 2004 Mar 25. PMID: 15089354.
16. Xu K. Gas-Kinetic Scheme for Unsteady Compressible Flow Simulations. von Karman Institute for Fluid Dynamics Lecture Series, Vol. 1998-03. von Karman Institute; 1998.
17. Li XM, Leung RCK, So RMC. One-step aeroacoustics simulation using lattice Boltzmann method. *AIAA J*. 2006;44:78-89.
18. Li XM. Computational Aeroacoustics Using Lattice Boltzmann Model. PhD thesis. Mechanical Engineering Department, Hong Kong Polytechnic University; 2006.
19. Eucken A. Über das Wärmeleitvermögen, die spezifische Wärme und die innere Reibung der Gase. *Physikalische Zeitschrift*. 1913;14:324-332.
20. Lallemand P, Luo LS. Theory of the lattice Boltzmann method: acoustic and thermal properties in two and three dimensions. *Phys Rev E Stat Nonlin Soft Matter Phys*. 2003 Sep;68(3 Pt 2):036706. doi: 10.1103/PhysRevE.68.036706. Epub 2003 Sep 23. PMID: 14524925.
21. Chen Y, Ohashi H, Akiyama M. Thermal lattice Bhatnagar-Gross-Krook model without nonlinear deviations in macrodynamic equations. *Phys Rev E Stat Phys Plasmas Fluids Relat Interdiscip Topics*. 1994 Oct;50(4):2776-2783. doi: 10.1103/physreve.50.2776. PMID: 9962315.
22. McNamara GR, Garcia AL, Alder BJ. Stabilization of thermal lattice Boltzmann models. *J Statistical Phys*. 1995;81:395-408.
23. Teixeira C, Chen H, Freed DM. Multi-speed thermal lattice Boltzmann method stabilization via equilibrium under-relaxation. *Comput Phys Commun*. 2000;129:207-226.
24. Shan X. Simulation of Rayleigh-Bénard convection using a lattice Boltzmann method. *Phys Rev E*. 1997;55:2780-2788.
25. Leung RCK, Kam EWS, So RMC. Recovery of the transport coefficients in the Navier-Stokes equations from the modeled Boltzmann equation. *AIAA J*. 2007;45:737-739.
26. Aristov VV. Direct Methods for Solving the Boltzmann Equation and Study of Nonequilibrium Flows. Kluwer Academic Publishers; 2001. Chapter 7.
27. So RMC, Leung RCK, Kam EWS, Fu SC. Progress in the development of a new lattice Boltzmann method. *Computers & Fluids*. 2019;190:440-469.
28. Fu SC, So RMC, Leung RCK. Modeled Boltzmann equation and its application to direct aeroacoustics simulation. *AIAA J*. 2008;46:1651-1662.
29. So RMC, Leung RCK, Fu SC. Modeled Boltzmann equation and its application to shock-capturing simulation. *AIAA J*. 2008;46:3038-3048.
30. So RMC, Fu SC, Leung RCK. Finite Difference Lattice Boltzmann Method for Compressible Thermal Fluids. *AIAA J*. 2010;48(6):1059-1071.
31. Lele SK. Direct numerical simulations of compressible turbulent flows: fundamentals and applications. In: Hanifi A, et al., editors. *Transition, Turbulence and Combustion Modeling*. Kluwer Academic Publishers; 1998. pp. 424-429.
32. Brenner H. Kinematics of volume transport. *Physica A*. 2005;349:11-59.
33. Brenner H. Navier-Stokes revisited. *Physica A*. 2005;349:60-132.
34. Greenshields CJ, Reese JM. The structure of shock waves as a test of Brenner's modifications to the Navier-Stokes equations. *J Fluid Mech*. 2007;580:407-429.
35. Kam EWS, So RMC, Leung RCK. Lattice Boltzmann method simulation of aeroacoustics and nonreflecting boundary conditions. *AIAA J*. 2007;45:1703-1712.
36. Li XM, So RMC, Leung RCK. Propagation speed, internal energy and direct aeroacoustics simulation using lattice Boltzmann method. *AIAA J*. 2006;44:2896-2903.
37. Leung RCK, Li XM, So RMC. Comparative Study of Nonreflecting Boundary Condition for One-Step Duct Aeroacoustics Simulation. *AIAA J*. 2006;44:664-667.
38. Tam CKW, Webb JC. Dispersion-relation-preserving finite difference schemes for computational aeroacoustics. *J Comput Phys*. 1993;107:262-281.
39. Gilbarg D, Paolucci D. The structure of shock waves in the continuum theory of fluids. *J Rat. Mech. Anal.* 1953;2:617-642.
40. Ohwada T. Structure of normal shock waves: direct numerical analysis of the Boltzmann equation for Hard-sphere molecules. *Phys Fluids A*. 1993;5:217-234.
41. Alsmeyer H. Density profiles in argon and nitrogen shock waves measured by the absorption of an electron beam. *J Fluid Mech*. 1976;74:497-513.
42. Thomas LH. Note on Becker's theory of the shock front. *J Chem Phys*. 1944;12:449-453.
43. Chu CK. Kinetic-theoretic description of the formation of a shock wave. *Phys Fluids*. 1965;8:12-22.
44. Bird GA. *Molecular Gas Dynamics and the Direct Simulation of Gas Flows*. Clarendon Press; 1994.
45. Yang JY, Huang JC. Rarefied flow computations using nonlinear model Boltzmann equations. *J Comput Phys*. 1995;120:323-339.
46. Xu K, Tang L. Nonequilibrium Bhatnagar-Gross-Krook model for nitrogen shock structure. *Phys Fluids*. 2004;16:3824-3827.
47. Xu K, Josyula E. Gas-kinetic scheme for rarefied flow simulation. *Math Comput Simul*. 2006;72:253-256.
48. Weiss W. Continuous shock structure in extended thermodynamics. *Phys Rev E*. 1995;52:R5760-5763.

INSTRUCTIONS FOR AUTHORS

IgMin Research | STEM, a Multidisciplinary Open Access Journal, welcomes original contributions from researchers in **S**cience, **T**echnology, **E**ngineering, and **M**edicine (STEM). Submission guidelines are available at www.igminresearch.com, emphasizing adherence to ethical standards and comprehensive author guidelines. Manuscripts should be submitted online to submission@igminresearch.us.

For book and educational material reviews, send them to STEM, IgMin Research, at support@igminresearch.us. The Copyright Clearance Centre's Rights link program manages article permission requests via the journal's website (<https://www.igminresearch.com>). Inquiries about Rights link can be directed to info@igminresearch.us or by calling +1 (860) 967-3839.

<https://www.igminresearch.com/pages/publish-now/author-guidelines>

APC

In addressing Article Processing Charges (APCs), IgMin Research: STEM recognizes their significance in facilitating open access and global collaboration. The APC structure is designed for affordability and transparency, reflecting the commitment to breaking financial barriers and making scientific research accessible to all.

IgMin Research - STEM | A Multidisciplinary Open Access Journal fosters cross-disciplinary communication and collaboration, aiming to address global challenges. Authors gain increased exposure and readership, connecting with researchers from various disciplines. The commitment to open access ensures global availability of published research. Join IgMin Research - STEM at the forefront of scientific progress.

<https://www.igminresearch.com/pages/publish-now/apc>

WHY WITH US

IgMin Research | STEM employs a rigorous peer-review process, ensuring the publication of high-quality research spanning STEM disciplines. The journal offers a global platform for researchers to share groundbreaking findings, promoting scientific advancement.

JOURNAL INFORMATION

Journal Full Title: **IgMin Research-STEM** | A Multidisciplinary Open Access Journal

Journal NLM Abbreviation: IgMin Res

Journal Website Link: <https://www.igminresearch.com>

Category: Multidisciplinary

Subject Areas: **S**cience, **T**echnology, **E**ngineering, and **M**edicine

Topics Summation: 173

Organized by: IgMin Publications Inc.

Regularity: Monthly

Review Type: Double Blind

Publication Time: 14 Days

Google Scholar: <https://www.igminresearch.com/gs>

Plagiarism software: iThenticate

Language: English

Collecting capability: Worldwide

License: Open Access by **IgMin Research** is licensed under a Creative Commons Attribution 4.0 International License. Based on a work at **IgMin Publications Inc.**

Online Manuscript Submission:
<https://www.igminresearch.com/submission> or can be mailed to submission@igminresearch.us